AD-A269 250

‖‖‖‖‖‖‖‖‖‖‖‖‖‖‖‖‖

Form Approved
OMB No. 0704-0188

Public reporting burden for this collection of information, including the time for reviewing instructions, searching existing data sources, gathering and maintaining the data needed, and completing and reviewing the collection of information. Send comments regarding this burden estimate or any other aspect of this collection of information, including suggestions for reducing this burden, to Washington Headquarters Services, Directorate for Information Operations and Reports, 1215 Jefferson Davis Highway, Suite 1204, Arlington, VA 22202-4302, and to the Office of Management and Budget, Paperwork Reduction Project (0704-0188), Washington, DC 20503.

1. AGENCY USE ONLY (Leave blank)	2. REPORT DATE 19 Aug 93	3. REPORT TYPE AND DATES COVERED Final Report 1/24/86 - 11/14/91

4. TITLE AND SUBTITLE The Intelligent Processing of Materials	5. FUNDING NUMBERS 5636/00 62712E

6. AUTHOR(S)
Brian G. Kushner

7. PERFORMING ORGANIZATION NAME(S) AND ADDRESS(ES) The BDM International, Inc. 7915 Jones Branch Drive McLean, VA 22102-3396	8. PERFORMING ORGANIZATION REPORT NUMBER

9. SPONSORING/MONITORING AGENCY NAME(S) AND ADDRESS(ES) AFOSR/NC Building 410, Bolling AFB DC 20332-6448	10. SPONSORING/MONITORING AGENCY REPORT NUMBER F49620-86-C-0036

11. SUPPLEMENTARY NOTES

12a. DISTRIBUTION/AVAILABILITY STATEMENT APPROVED FOR PUBLIC RELEASE; DISTRIBUTION IS UNLIMITED.	12b. DISTRIBUTION CODE

13. ABSTRACT (Maximum 200 words)

See Attached

DTIC
ELECTE
SEP 0 9 1993
S A D

14. SUBJECT TERMS		15. NUMBER OF PAGES 52
		16. PRICE CODE

17. SECURITY CLASSIFICATION OF REPORT UNCLASSIFIED	18. SECURITY CLASSIFICATION OF THIS PAGE UNCLASSIFIED	19. SECURITY CLASSIFICATION OF ABSTRACT UNCLASSIFIED	20. LIMITATION OF ABSTRACT

NSN 7540-01-280-5500

Standard Form 298 (Rev. 2-89)
Prescribed by ANSI Std. 239-18
298-102

13. This report covers progress in novel concepts for the development and implementation of Intelligent Processing of Materials (IPM) in the production of advanced materials, with special emphasis on defense applications.

IPM is inherently a multidisciplinary effort, combining the latest in materials processing knowledge in the form of process models, novel, in-situ process sensors, and emerging control theory for adaptive control of highly nonlinear processes. The concepts reported below have been studied to assess their value in streamlining the development of new methods for establishing regions of process variable space which are inherently stable, thereby reducing the laborious and experimentally intensive task of process design for production of advanced materials, and to a distributed simulation environment known as the Virtual Factory for rapid prototyping of intelligent control systems, which was originally developed in a parallel research project sponsored by ARPA through NIST. Finally, these new techniques, concepts and capabilities have been applied to the processing of advanced materials for military applications, including near net shape forming of titanium alloy powders to form shaped parts representative of gas turbine engine components, and the growth of single crystal infrared detector materials based upon calmium zinc telluride, which is the substrated material for infrared focal plane arrays. These efforts have been conducted by BDM scientists and engineers, in conjunction with leading university research from MIT and the University of California, Santa Barbara (UCSB).

BDM

BDM INTERNATIONAL, INC.
4001 NORTH FAIRFAX DRIVE
SUITE 750
ARLINGTON, VA 22203
(703) 351-6900

THE INTELLIGENT PROCESSING OF MATERIALS

FINAL TECHNICAL REPORT

Sponsored by
Advanced Research Projects Agency
ARPA Order No. 5636
Monitored by AFOSR Under Contract No. F49620-86-C-0036

AUGUST 19, 1993

The views and conclusions contained in this document are those of the authors and should not be interpreted as necessarily representing the official policies or endorsements, either expressed or implied, of the Advanced Research Projects Agency or the U. S. Government.

BDM FEDERAL, INC.

I. REPORT SUMMARY

This report covers progress in novel concepts for the development and implementation of Intelligent Processing of Materials (IPM) in the production of advanced materials, with special emphasis on defense applications.

IPM is inherently a multidisciplinary effort, combining the latest in materials processing knowledge in the form of process models, novel, in-situ process sensors, and emerging control theory for adaptive control of highly nonlinear processes. The concepts reported below have been studied to assess their value in streamlining the development of new methods for establishing regions of process variable space which are inherently stable, thereby reducing the laborious and experimentally intensive task of process design for production of advanced materials, and to a distributed simulation environment known as the Virtual Factory for rapid prototyping of intelligent control systems, which was originally developed in a parallel research project sponsored by ARPA through NIST. Finally, these new techniques, concepts and capabilities have been applied to the processing of advanced materials for military applications, including near net shape forming of titanium alloy powders to form shaped parts representative of gas turbine engine components, and the growth of single crystal infrared detector materials based upon cadmium zinc telluride, which is the substrated material for infrared focal plane arrays. These efforts have been conducted by BDM scientists and engineers, in conjunction with leading university researchers from MIT and the University of California, Santa Barbara (UCSB).

Accesion For		
NTIS CRA&I	☑	
DTIC TAB	☐	
Unannounced	☐	
Justification		
By		
Distribution /		
Availability Codes		
Dist	Avail and / or Special	
A-1		

BDM FEDERAL, INC.

II. TECHNICAL RESULTS

A. Intelligent Processing of Materials (IPM) Concepts

TOPIC 1: RAPID INTELLIGENT CONTROLLER PROTOTYPING UTILIZING A DISTRIBUTED PROCESS FOR THE DESIGN, DEVELOPMENT AND EXECUTION OF DISTRIBUTED SIMULATIONS

Jeffery Payne and Richard Mills, BDM International

BDM has developed multi-workstation based simulation environment to enable the rapid prototyping of Intelligent Control Systems. This environment encompasses models for materials processes, models of processing equipment and sensors, and sensor data analysis models. The models are distributed on multiple workstations, which have to be coordinated for use in prototyping intelligent control systems.

A distributed process manager (DMAN) developed to aid the design, development and execution of distributed simulations. DMAN provides both a set of interprocess communication (IPC) libraries for communication between distributed clients, and an environment which allows client processes to be dynamically linked and executed on a network of workstations. DMAN has been developed to allow client processes to execute on any assigned workstation while displaying their graphical user interface (GUI) either locally or remotely on any other display in the system. By providing these capabilities, DMAN has proven useful as a flexible environment in which distributed applications (particularly simulations) can be more easily designed, developed, and executed. DMAN has been used to successfully build both a manufacturing system simulation for HIP and for crystal growth.

Executing a simulation in a distributed processor environment -- where the simulation is split into concurrently executing *simulation client processes* which communicate over a connected network -- has several advantages over execution on a traditional sequential processor. Simulations executed in this manner are called *distributed simulations* and have an obvious potential for simulation speed up due to the concurrent execution of their simulation algorithms.

Another advantage of distributed simulation is the relative ease by which individual simulation processes can be modified or even replaced without drastic modification to the rest of the simulation. By restricting all communication between simulation processes to messages passing, the internal computational algorithms associated with any given simulation process can be modified or even replaced without simulation-wide affects, as long as the message communication to the other processes remains the same[1]. A final advantage of distributed simulation is the ability

to optimize the design, development, and execution of distributed computations irrespective of the other processes in the simulation. By separating simulations into distributed client processes, it is easy to design and develop individual client processes in the environment (interface, language, development tool) most conducive to development. This also allows each simulation process to execute on the processor platform most suited for its computation, using standard message passing to communicate with the rest of the simulation.

Unfortunately, along with the advantages of distributed simulation come many problems. Fundamental characteristics of computation which exist in sequential processing often no longer exist when moving to a distributed environment[3][1][5][2]. These characteristics include: a globally accessible shared memory space, a global representation of time, information regarding physical addresses of program locations, atomic access to operations and variables, and deterministic execution of simulation algorithms. Each of these characteristics must be addressed by a distributed system in order to assure correct execution of simulations. Typically some of these characteristics are encompassed by a particular hardware configuration while others are maintained in software. For example, a shared memory parallel processor maintains both a globally accessible shared memory and also a global clock. It does not, however, provide atomic access to a set of memory locations or automatically execute concurrent tasks. If atomic access or automatic task execution are necessary than these features must either be provided by the system software or designed into the simulation proper.

Besides the issues associated with concurrent execution of tasks and atomic access to memory locations, distributed simulations must have a mechanism for the assignment, spawning, and reaping of all simulation clients. Often such mechanisms are application specific, designed solely to allow a given application to execute on a network of processors. While adequate for a single application, such an approach does not provide a general purpose methodology for creating simulations that can easily be modified, reconfigured, or moved to a new platform without extensive redevelopment or redesign. Other systems provide adequate spawning and reaping facilities but do not allow application developers to assign particular simulation clients to particular processors. Although this approach is general purpose, it is often too general for realworld applications. Typically it is desired to assign at least one simulation client within a distributed simulation to a specific processor. This is often desirable either because a particular simulation client is optimized for a given processor or because the simulation needs the graphics capabilities of a particular workstation.

In order to provide a useful distributed environment for distributed simulation within a network of workstations, the author's have developed the Distributed Process Manager (DMAN)

package. DMAN is a X Window System$^{(TM)}$ based tool for the dynamic definition. connection, and execution of distributed simulations. Distributed simulation processes are built to execute within DMAN using a set of communication libraries which provide high level message passing constructs for communication with other simulation processes and with DMAN itself. The libraries provide both reliable TCP/IP network communication and RS-232 serial communication between any two connected processes. By abstracting away the low level details of process communication, all simulation processes do not need to know with whom they are communicating or over what type of network link. Removing such details from simulation processes allows distributed application developers to connect and execute any number of system simulations by dynamically connecting simulation processes and then executing the application using DMAN's facilities. DMAN also allows application developers to dynamically specify the host machines for both execution and display of simulation process output (X Window interfaces). By managing the assignment of processes to processors a distributed application developer can take advantage of machine specific optimizations for particular algorithms within the simulation. For example, if one were including a finite element method (FEM) analysis process as part of a simulation, one would wish to execute this very computational algorithm on a very fast sequential processor or even a parallel processor to remove the computational bottleneck of FEM analysis from the simulation. Similarly, algorithms or models which require intensive graphics processing for their interface will benefit by executing on a high performance graphics workstation. In this manner distributed applications can be developed that take advantage of machine specific optimizations for some simulation processes without the need to develop the entire application on a specific platform .

DMAN has proved successful at both speeding up application development in developing IPM control systems and providing a flexible, fast environment in which to design distributed applications. The environment is most applicable for applications which require constant reconfiguration and which need to use specific processor/display hardware for optimization of simulation clients. By removing the requirement that simulation clients know where they are executing and with whom they are communicating, DMAN provides an environment which allow dynamic reconfiguration of applications without recompilation of simulation client source code.

The Virtual Factory (VF) concept envisions a virtual environment in which closed-loop process control software systems and scenarios can be successfully tested and executed without the use of actual manufacturing equipment. Instead, the control software interacts with a suite of software models which accurately simulate both factory equipment and the manufacturing processes within the system. The virtual factory concept has been implemented at BDM and is

currently used to prototype and develop closed-loop control systems for various manufacturing environments.

The distributed process manager (DMAN) previously described is at the heart of the virtual factory. VF applications are built, spawned, executed, and reaped all under DMAN. By intelligently allocating simulations to machines most suited for their execution (based upon speed, special graphics capabilities, etc.), DMAN provides a means of executing VF applications quickly and easily. In addition, DMAN provides the communication and information necessary to allow generic simulation models to seamlessly connect to their peers with any defined communication interface. All communication between the Distributed Process Manager and the simulation models is done through transparent socket network communications. The users and developers of VF models are never aware of this communication. All virtual factory applications have been developed within DMAN and use the X Window System™ for graphical output of simulation information. DMAN allows a virtual factory application designer to pick and choose factory equipment simulations and connect these simulations into a manufacturing system in any configuration that makes physical sense. This is done by providing -- for each different equipment simulation -- only those interfaces common to the hardware it is simulating. Work is ongoing to include various types of interface connections and provide a representative suite of equipment models for factory simulation.

The design and development of process control software (controllers) is a difficult task. Besides the implementation issues inherent in controller development (e.g. event scheduling, real-time processing, user interface updating, algorithm selection), there are many other problems that must be addressed. These problems include:

1.   *lack of production equipment:* it is often difficult to take production equipment "off-line" in order to test and debug new control approaches,

2.   *location of production equipment:* seldom is production equipment easily accessed by the developers of control systems,

3.   *safety:* faulty control software being tested on actual manufacturing equipment can result in catastrophic failure of the system resulting in both injury and equipment destruction,

4.   *component interface issues:* often while integrating new manufacturing hardware and a new controller into a manufacturing environment the problems encountered

have more to do with connectivity between hardware and software components than the control software itself, and

5. *speed:* the speed of many manufacturing processes are too slow to allow rapid test and debugging of software control systems.

In order to address these concerns, BDM has developed a concept called the Virtual Factory (VF). This concept envisions a virtual manufacturing environment in which closed-loop process control software can be successfully designed, developed, tested, and executed within a typical office environment. This concept uses software simulations of both manufacturing equipment and process models in order to simulate closed-loop manufacturing systems.

VF CONCEPT: The virtual factory concept attempts to reduce the number of issues associated with software controller development by eliminating all hardware components from a manufacturing environment during a controller's design, development, test, and analysis. This is achieved by developing software simulation models which are capable of simulating all hardware components in a given manufacturing system and also all manufacturing processes within the system.

In order to provide the control system developer with an environment which closely simulates that of the actual manufacturing system, each simulation model is a separate executing client simulation process which communicates with its neighboring simulation clients through standard communication protocols. This approach allows generic hardware and process simulations to be executed irrespective of other client simulations within the environment, thus providing a means of easily reconfiguring a manufacturing environment by simply swapping out selected client simulations for others. The control system communicates with the VF through standard communication interfaces such that the controller never knows whether it is processing information for an actual manufacturing line or the virtual factory. This approach allows the developer of a control system to easily move a software controller from the virtual factory to an actual manufacturing environment without modification of the controller.

In essence, the VF solves many of the problems mentioned in the introduction: no manufacturing equipment is needed for controller development (takes no production equipment off-line and removes the need to relocate software developers close to the manufacturing system), no safety issues since all equipment is virtual and cannot cause physical harm, interface issues can be resolved in stages to assure that hardware/software interfaces will not be a problem when configuring a new manufacturing system, and execution of the simulations is typically fast enough to allow quick test and analysis of complex manufacturing processes. In addition to addressing

BDM FEDERAL, INC.

these problems, the virtual factory also has other advantages over traditional development environments for controllers:

1. the VF c   reconfigured to contain other factory equipment and other process models without additional hardware costs and in rapid fashion,

2. the system can act as a testbed for the development of manufacturing process models which simulate manufacturing processes, and

3. commercial off-the-shelf (COTS) software can be integrated into the system in order to allow standard modeling and interface packages to be included within the VF.

IMPLEMENTATION: BDM has realized the concept of the Virtual Factory through the development of component models capable of simulating both manufacturing hardware and manufacturing processes. The work has focused on modeling and simulating closed-loop control of the Hot Isostatic Pressing (HIP) process. The HIP process takes a powdered material and exposes it to high temperatures and pressures during a long (sometimes 6-10 hour) process. The goal of the process is to heat and pressurize the material until desired material properties (near net shape, high densification) are obtained. For a given set of materials, the HIP process is capable of producing very dense, strong material useful in component design.

A typical closed-loop control environment for the HIP process may include:

•   the software controller which controls the process by providing temperature (T) and pressure (P) schedules to the system to control HIP furnace interaction with the material,

•   an actuation controller for controlling the heating zones in the HIP furnace based upon T and P schedules sent from the software controller,

•   a HIP furnace which processes material located within its chamber,

•   sensors to detect changes in the material's size, density, etc.,

•   data acquisition equipment to read these changes and send information back to the control system.

BDM has developed simulation models which realize the virtual factory concept for HIP processing. These models simulate both the above manufacturing equipment and the process

model associated with densification of material. This implementation has been used to prototyping actual control systems for the HIP process. Some of these prototypes are currently being developed into industrial controllers for actual manufacturing systems.

The Virtual Factory currently operates in a distributed environment consisting of high performance Sun SPARC workstations. The environment allows all component simulations of hardware and models to execute concurrently on selected machines within the network.

VF Models: There are many models currently implemented within the virtual factory. These include both hardware simulators and process simulators. The equipment simulators include:
1. actuation equipment - A/D and D/A equipment which either sends or receives information from the HIP chamber.
2. sensor models - models the of in-situ sensors located within the HIP chamber, and
3. HIP chamber models - models of the physical conditions inside the HIP chamber.

CONCLUSIONS: The development of the virtual factory has addressed many concerns regarding software controller development. It has proved useful in the prototyping of control systems and also the development of process and sensor models. By allowing each simulation within the system to execute independently, the system has exhibited high speeds and also proved to be very flexible in terms of reconfiguration of prospective manufacturing environments.

TOPIC 2: NONLINEAR SYSTEMS STABILITY ANALYSIS APPLIED TO INTELLIGENT PROCESSING OF MATERIALS

Stuart B. Brown, MIT; Norman M. Wereley and John J. Wlassich, BDM International

Intelligent control of materials processing is based upon the development and application of advanced mathematical techniques to deal with highly nonlinear processes. Current control techniques are limited to linearization techniques which are subject to loss of critical information with regard to prediction of inherent process stability envelopes. This study applies special mathematical techniques to assist the process designer in establishing process regimes which do no suffer from microstructural instabilities such as dynamic recrystallization or runaway grain growth.

Control of consolidation and deformation processing (e.g., by hot isostatic pressing (HIP), forging, extrusion, superplastic forming) is predicated on defining stable control regimes in material behavior that determine the range of processing variables, such as temperature and

BDM FEDERAL, INC.

deformation rate. Constitutive models that couple flow and microstructure evolution can be expressed by internal variable models consisting of systems of coupled, first order, nonlinear ordinary differential equations. Given this mathematical form, the stability of these models may be analyzed using analytical techniques applied in nonlinear controls and systems theory. BDM and MIT have employed Lyapunov's direct method to analytically determine processing regimes that avoid dynamic recrystallization, a material instability occurring in rate dependent materials during hot deformation.

Nonlinear stability analysis offers distinct advantages over linear approximation techniques. The nonlinear approach yields results that are global in scope, rather than local. as in the case for linear approximation methods. In addition, nonlinear analysis involves less abstraction from actual physical material processes. Nonlinear techniques are directly applicable to the design of nonlinear control algorithms. The material systems can therefore be coupled to the control of microstructure and instabilities through nonlinear control system design procedures.

The desire to incorporate the effect of material microstructure on deformation behavior has motivated the development of internal variable constitutive models for flow. These models of rate-dependent, multiaxial flow have become increasingly complex, incorporating highly nonlinear flow and evolution equations that depend on scalar and tensorial structure variables. Representative internal variables models include those for metal flow [3, 4, 10], polymers [1], and multiphase systems [2]. These internal variable deformation models usually consist of a set of coupled flow and evolution equations of the form:

$$\frac{d\varepsilon_{ij}^{vp}}{dt} = \hat{f}_{ij}(\sigma_{kl}, T, s_1, \ldots, s_m)$$

where

ε_{ij}^{vp}	=	Viscoplastic strain,
$\hat{f}_{ij}(\ldots)$	=	flow function.
σ_{kl}	=	state of stress,
T	=	temperature,
$s_1, \ldots, s_m$	=	list of m internal variables, and
$\hat{g}_n(\ldots)$	=	evolution equation for internal variable n.

The internal variables s_n may be scalars of higher order, even-ranked tensors [7].

The general form of these equations is analogous to that used within the control and systems analysis communities for the characterization of dynamic systems. Dynamical models are

9

frequently represented via a state-space formulation with the system dynamics captured by a system of first-order differential equations that can be both nonlinear and highly coupled. If we define a state vector

$$x = \{X_1, X_2, X_3, ...\}$$

then the time history of this system is modeled by a set of dynamic functions

$$\frac{dx}{dt} = \hat{x} = \hat{X}(x).$$

In this case we have assumed that the system dynamics are not dependent on time.

Once a particular system is modeled using the state-space formalism, a collection of analytical methods (phase plane representation, perturbation methods, bifurcation analysis, Lyapunov stability) [6,5] become available to investigate the dynamics of that system model.

Lyapunov's method represents a special case of summarizing functions to explore the behavior of a dynamical system. We define a summarizing functions as a scalar function of the system state vector x.

The variation of the summarizing function with time is then used to represent aspects of the behavior of the aggregate system. If we define an equilibrium point to be a state vector that, once reached, does not change, i.e., from Equation 4

$$0 = \hat{X}(x)$$

then Lyapunov analysis permits examination of the stability of that equilibrium point.

The formal statement of stability based on Lyapunov's direct method can be stated in terms of an equilibrium point at the origin[1]:

THEOREM: Let x*(t) = 0, t≥ t$_0$, to be the zero solution of the regular system $\dot{x} = \hat{X}(x)$, where $\hat{X}(0) = 0$. Then x*(t) is uniformly stable for t ≥ t$_0$ if there exists V (x) with the following properties in some neighborhood of x - 0:

1. V(x) and its partial derivatives are continuous;
2. V(x) is positive definite;
3. $\dot{V}$ is negative semidefinite.

BDM FEDERAL, INC.

The implication is that if one can define a Lyapunov function for a given equilibrium point, then the equilibrium point is stable and the domain where the summarizing function V(x) is a valid Lyapunov function represents a domain of stability for that point. It is important to note that a Lyapunov function is not unique. The domain of stability depends on the particular Lyapunov function selected.

Lyapunov stability analysis can be used in a design sense to define parameters or operating conditions that guarantee stable behavior - i.e., where that state variable will remain with a given region in state space. For intelligent processing applications one can ascertain processing limits where, if the process remains within these limits, one can predict the onset of instability, such as recrystallization.

REFERENCES:

[1]   M. C. Boyce, D. M. Parks, and A. S. Argon. Plastic flow in oriented glassy polymers. *International Journal of Plasticity*, 5(6):593-615, 1989.

[2]   S. B. Brown. An internal variable constitutive model for the thixotropic behavior of metal semi-solid slurries. In *Materials Science Seminar of Intelligent Processing of Materials*, American Society of Metals, October 1989.

[3]   S. B. Brown, K. H. Kim, and L. Anand. An internal variable constitutive model for the hot working of metals. *International Journal of Plasticity*, 5(2):95-130, 1989.

[4]   E. P. Cernocky and E. Krempl. Evaluation of a uniaxial, nonlinear second-order differential overstress model for rate-dependence, creep and relaxation. *International Journal of Solids and Structures*, 19(9):753-766, 1983

[5]   D. W. Jordan and P. Smith. *Nonlinear Ordinary Differential Equations*. Claredon Press, 1987.

[6]   D. Luenberger. *Introduction of Dynamic Systems*. John Wiley & Sons, 1979.

[7]   E. T. Onat. Representation of elastic-plastic behavior in the presence of deformations and anisotropy. In *Topics in Plasticity*, pages 45-71, 1991.

[8]   T. Sakai and J. J. Jonas. Dynamic recrystallation: mechanical and microstructural considerations. *Acta Metallurgica*, 32(2):180 - 209, 1984.

[9] C. M. Sellars. Modeling of structural evolution during hot working processes. In *Annealing Processes. Recovery, Recrystallization and Grain Growth, 7th Risco International Symposium on Metallurgy and Materials Science*, pages 167 - 187, *1986*.

[10] D. C. Stougger and S. R. Bodner. A constitutive model for the deformation induced anisotropic plastic flow of metals. *International Journal of Engineering Science*, 17(6):757-764, 1979.

B. Case Studies: Intelligent Processing of Advanced Materials for Defense Applications

TOPIC 1: DEVELOPMENT OF MICRO MECHANICS · BASED, MECHANISTIC CONSTITUTIVE LAWS FOR FINITE ELEMENT METHOD (FEM) MODELING OF THE CONSOLIDATION OF POWDER MATERIALS BY HOT ISOSTATIC PRESSING (HIP)

Dr. T. F. Zahrah, BDM International, and L. T. Kuhn and R. M. McMeeking, University of California, Santa Barbara (UCSB)

In response to the need for describing a powder aggregate densifying under nonhydrostatic stress. a number of constitutive laws for arbitrary stress states have recently been derived. This report summarizes the results of the mechanism-based modeling efforts which have addressed both Stage I (when the powder particles meet at small isolated contacts and the porosity is interconnected) and Stage II (when only isolated spherical pores remain). The results are appli. ble to powders densifying by plasticity, diffusional and power-law creep mechanisms. The new models reduce to the established equations for hydrostatic compaction with no deviatoric stresses and are presented so that they may easily be incorporated into numerical schemes.

INTRODUCTION

Ashby and coworkers [1,2] have establish models for densification of powder aggregates under pure hydrostatic stress. The models for individual mechanisms leading to or inhibiting densification have been verified and then integrated within computer software so as to be displayed in the form of a densification map, as illustrated in Figure 1. The maps have been successfully

BDM FEDERAL, INC.

applied to the design of Hot Isostatic Pressing (HIP) consolidation cycles. In addition to hydrostatic stresses, non-hydrostatic stress fields are known to arise during HIP from the shielding effect of the powder container, from density and temperature gradients within the sample and during composite consolidation. This necessitates the inclusion of deviatoric stresses in the powder constitutive laws to further optimize HIP cycles. In addition, generalization of the laws to arbitrary stress states increases their applicability to a wider variety of processing techniques including uniaxial pressing, hot rolling, and sintering. The laws in this form can also be used for deformation modeling of incompletely pressed products made by powder metallurgy.

THE MECHANISM-BASED APPROACH

The Deformation Mechanisms and Regimes

The primary deformation mechanisms during HIP are identified as plasticity, diffusional and power-law creep by Helle et al. [1] and Ashby [2,3] and are modeled for both Stage I and Stage II. In Stage I, the macroscopic deformation is controlled by particle deformation at the contacts. The unit problem in this case is the interaction between two particles across a contact area. In stage II, removal or expansion of isolated porosity controls the deformation and hence a spherical pore is the unit cell. In the micromechanics-based approach the response of the aggregate of particles is derived from the response of the unit cell. The derivation is repeated for each densification mechanism. As a result, the models are referred to as micromechanics, mechanism-based models.

McMeeking and co-workers [4,5,6,7] adopted a number of the assumptions that were made in the development of the models derived for pure hydrostatic stress so that the constitutive laws could be generalized simply by including a shear analysis in the existing mechanism-based approach. Most importantly they stipulated that the new models reduce to the hydrostatic results which have been extensively validated for HIP.

Flow Potential and Flow Law

To characterize the Stage I laws for non-hydrostatic stress states virtually the same procedure is followed for each deformation mechanism. The analysis consists of specifying the macroscopic strain rate in the powder aggregate and computing the normal and shear energy dissipated by the unit deformation mechanism. The work rate is used in a potential Ψ to determine the macroscopic deformation parameters. The individual components of strain rate are then related to those of stress, σ_{ij}, by

$$\dot{\varepsilon}_{ij} = \lambda \frac{\partial \psi}{\partial \sigma_{ij}} \tag{1}$$

13

where λ is a multiplier. For power-law and diffusional creep, $\lambda = 1$ whereas for plasticity, λ must be determined by consistency and kinematics. This is a flow law defining the strain rate vector as the gradient of the scalar potential which is usually a function of the stress alone.

The characterization of Stage II laws proceeds from a different considerations than for Stage I. The macroscopic behavior of a deforming powder in Stage II is modeled by the response of a sphere of material containing a concentric spherical void. Axisymmetric states of macroscopic stress are applied to the unit cells ranging from purely hydrostatic to purely deviatoric loading. The results are presented in terms of a potential function Ψ and the macroscopic components of strain are again given by Eq. (1)

STAGE I MODELS FOR NON-HYDROSTATIC STRESS STATES

The axisymmetric deformation of a macroscopic randomly packed isotropic element of powder compact depicted in Figure 2 was considered to derive the Stage I constitutive laws [4,5,6]. In the random close packed configuration (D=0.64 for monosized spheres) the particles make point contact with each other and there is no room in the interparticle space to accommodate another particle without deformation. During the deformation necessary for consolidation, the powder is considered to continue to resemble this configuration except for a flattening of the contacts. The models have been developed by assuming the particles remain bonded and the particle centers move compatibly with the macroscopic strain rate. As a result, the constitutive laws which result typically bound from above the true behavior in terms of stress.

Plastic Yielding

The slip line field from Green [8] for a junction under combined shear and normal loading provides the local contact stresses required to compute the internal dissipation from plastic yielding. The yield surface values are normalized by the yield pressure for pure hydrostatic stress [1]

$$P_y = 2.97\,\sigma_y D^2 \left(\frac{D - D_o}{1 - D_o} \right) \tag{2}$$

where σ_y is the yield stress in tension of the material composing the powder, D_o is the initial relative density, and D is the current relative density. The plasticity yield surface can be approximated for conditions of high pressure by

$$\psi_p^I = 2q / 3p_y - p / p_y - 1 = 0 \tag{3}$$

14

where q is the effective (or shear) stress and p is the hydrostatic pressure. The subscript indicates the mechanism (plasticity) and the superscript indicates the stage of densification (Stage I). This yield criterion, illustrated in Figure 3, shows that at high pressures the effective stress to cause yielding is linearly dependent on the applied pressure. As the macroscopic strain rate is normal to the yield surface and since there is a vertex on the yield surface (at $q = 0$), the strain rate for states of pure macroscopic pressure is somewhat arbitrary. That is the strain rate can range from pure macroscopic densification (through combinations of pressure and shear) to a uniaxial strain. The flow law for the powder compact can be developed from Eq. (1).

Power-Law Creep

The power-law creep constitutive law derivation proceeds as above from a calculation of the work rate of a unit cell requiring local stresses σ_{ij}. An analytical relation for the local stresses at a particle conta... due to combined pressure and shear was not immediately available for particles of a power-law material. As power-law creep is an important HIP mechanism, a detailed stress analysis of a small area of contact between two creeping particles was performed employing the ABAQUS finite element package

A steady state creep flow surface was obtained for a particle contact for stress exponents of $n = 1, 3, 5, 10$ and 100 [11]. The numerically obtained stresses are an estimate of those required to allow steady state shearing and normal flow of the particle centers relative to one another. The sharp vertex seen on a local level in the Green [8] plasticity slip line solution for a contact under combined shear and normal loading was softened to a region of high curvature for the power law material. The average stresses σ_n and σ_t obtained from the numerical calculations were used to compute the internal work rate. The results in the form of a macroscopic flow potential in p - q space are shown in Figure 4 along with results obtained from a preliminary computation which neglected the shear dissipation. The mean stress p and the effective stress q are normalized with respect to $C\sigma_0$ where σ_0 is a material parameter and C is defined as

$$C = \frac{9}{4}\left(\frac{8\sqrt{3}}{9\pi}\right)^{\frac{1}{n}} D^2 \left(\frac{D - D_o}{1 - D_o}\right)^{1-\frac{1}{2n}} \tag{4}$$

The results of the two calculations are seen to be nearly identical. The only difference is a softening of the high regions of curvature near the hydrostatic stress axis. Analytical expressions for the more precise potential were found to be prohibitively complicated for a small increase in accuracy. Therefore the more approximate results were determined to be an adequate solution for the HIP problem.

15

The power-law creep potential for non-nydrostatic compaction of a powder based on the contours in Figure 5 is

$$\psi_c^I = \frac{\dot{\varepsilon}_0 \sigma_0}{n+1} \frac{27\pi}{16\sqrt{3}} \left(\frac{D-D_0}{1-D_0}\right)^{\frac{1}{2}} \left\{ \frac{(1-D_0)}{3D^2(D-D_0)} \left[\left(\frac{|\Sigma_m|}{\sigma_0}\right)^{\frac{n+1}{n}} - \left(\frac{2\Sigma_e}{3\sigma_0}\right)^{\frac{n+1}{n}} \right] \right\}^n \quad (5)$$

where $\dot{\varepsilon}_0$ and σ_0 are the particle material creep parameters.

The generalized constitutive law for powder densification by power law creep is obtained by differentiation of the potential according to Eq. (1).

Diffusional Densification

The controlling process during linear creep of a Stage I powder compact is the diffusional transport of material from necks between particles to the free surfaces. McMeeking and Kuhn [5] developed a constitutive law for diffusional densification based on a diffusional particle to particle interaction. They assumed diffusion is very rapid on the free surface of the powder so that the critical phenomenon is mass transport on the interparticle boundary. An interparticle shear viscosity is allowed for also.

The macroscopic constitutive law which results is

$$\dot{\varepsilon}_{ij} = S_{ij} / 2\mu + (p - \sigma_s)\delta_{ij} / 3K \quad (6)$$

where σ_s is a term driving sintering. The sintering stress, normal and shear bulk viscosities are given by

$$\sigma_s = \frac{D^2(D-D_o)}{(1-D_o)}\left(\frac{D_o}{D}\right)^{\frac{1}{3}} \sigma_o \quad (7)$$

$$K^I = \left(\frac{D_o}{D}\right)^{\frac{2}{3}} \frac{D^2(D-D_o)^2 R_o^3}{36(1-D_o)^2 D} \quad (8)$$

$$\mu^I = \left(\frac{D_o}{D}\right)^{\frac{2}{3}} \frac{D^2(D-D_o)^2 R_o^3}{60(1-D_o)^2 D} \quad (9)$$

16

In these expressions σ_O and D are parameters controlling the mass transport of material into porosity away from contacts between powder particles and $2R_O$ is the diameter of the powder particles. The particle size enters because it sets the diffusion distances. The viscosities disappear at $D = D_O$ showing that it is very easy to deform the powder compact at low relative densities.

STAGE II MODELS FOR NON-HYDROSTATIC STRESS STATES

Each of the Stage II constitutive laws (isolated porosity) are characterized from the response of an isolated, closed spherical pore. The modified Gurson law [10,12] as proofed in Ashby's initial survey is presented in the section below for the Stage II plasticity regime. For the Stage II power-law creep regime the creep potential by Sofronis and McMeeking [7] is presented. The diffusion densification regime is modeled as a special case (n = 1) of the Sofronis and McMeeking power-law potential.

Plastic Yie'ding

The Richmond and Smelser [12] modification of the Gurson constitutive equation provides a superior description of non-hydrostatic Stage II compaction behavior. The yield potential, as proposed by Ashby [3] is

$$\left(\frac{q}{\sigma_y}\right)^2 + 2(1-D)\cosh\left(\frac{3p}{2\sigma_y}\right) - \left(1 + (1-D)^2\right) = 0 \tag{10}$$

Equation (10) reduces to the von Mises flow law $q = \sigma_y$ when $D = 1$ and to the Stage II HIP equation for hydrostatic compaction

$$p = \frac{2}{3}\sigma_y \log_e\left(\frac{1}{1-D}\right) \tag{11}$$

when $q = 0$.

The components of strain are found by differentiation of Eq. (10) as per Eq. (1).

Power-Law Creep

A constitutive law for the power-law creep of a material containing spherical voids (Stage II powder) was characterized from finite element cell calculations by Sofronis and McMeeking [7]. The macroscopic behavior of the material was modeled by the response of a sphere of material containing a concentric spherical void. This approach parallels that followed by Gurson to obtain the basis of the potential for plasticity (Eq. (10)). The potential for power law creep from Sofronis and McMeeking [7] is

$$
\psi_c^{II} = \frac{\sigma_o \dot{\varepsilon}_o}{n+1} \left\{ \left(\frac{2-D}{D} \right)^{\frac{2n}{n+1}} \left(\frac{q}{\sigma_o} \right)^2 + \left[\frac{(1-D)n}{\left[1-(1-D)^{\frac{1}{n}} \right]^n} \right]^{\frac{2}{n+1}} \left(\frac{3p}{2n\sigma_o} \right)^2 \right\}^{\frac{n+1}{2}} \tag{12}
$$

The flow surface in p - q space is shown in Figure 5 for $D = 0.90$. The creep rate found by differentiation of Ψ as per Eq. (1).

Diffusional Creep

The general form of the constitutive law for Stage II diffusional creep is given by Eq. (5) as well. The diffusional normal and shear viscosities K^{II} and μ^{II} for Stage II are obtained from the linear case ($n = 1$) of the Sofronis and McMeeking power law potential. With $\Sigma_S = 0$ they are

$$
\mu^{II} = \frac{\mu_o D}{2 - D} \tag{13}
$$

and

$$
K^{II} = \frac{4\mu_o D}{3(1 - D)} \tag{14}
$$

where μ_o is the shear viscosity of the material the spheres are composed of. The model has the right features, reducing to the prior Ashby solution at the limits of pure shear and pure hydrostatic compression.

CONCLUSIONS

Mechanism-based constitutive models have been developed for powder compaction under the combined effects of hydrostatic and deviatoric stresses. The models have the right features in

18

that they reduce to the well established HIP equations for pure hydrostatic pressure and agree well with the limited experimental data they have been compared to. However, further experimental verification of the models is required before they can be implemented with confidence in numerical codes for HIP or other material processing techniques.

An experimental verification program is currently underway replete with experiments at various densities for each deformation mechanism. Finite element calculations incorporating the models for Stage I and Stage II densification are expected to indicate the suitability of the generalized laws.

REFERENCES

1. Helle, A. S., K. E. Easterling and M. F. Ashby, *Acta Metall.*, **33** (1985) 2163.

2. Ashby, M. F., *HIP 6.0 Background Reading, Engineering Dept.*, (1990) Trumpington St., Cambridge CB2 1PZ, England.

3. Ashby, M. F., paper presented at the meeting for Powder Compaction Modeling BDM International, Arlington, VA. March 1990.

4. Fleck, N. A., L. T. Kuhn and R. M. McMeeking, to be published in J. *Mech. Phys. Solids, 1991.*

5. McMeeking, R. M. and L. T. Kuhn. "A Diffusional Creep Law for Powder Compacts," to be published in *Acta Metall. et Mater.*, 1991.

6. Kuhn, L. T., and R. M. McMeeking. "Power Law Creep of a Powder Compact Due to Combined Pressure and Shear," submitted to *Int. J. Mech. Sci,* 1991.

7. Sofronis, P. and R. M. McMeeking. "Creep of a Power Law Material Containing Spherical Voids," to be published in *J. App. Mech.*, 1990.

8. Green, A. P., *J. Mech. Phys. Solids.* **2** (1954) 197.

9. Hibbitt, Karlsson and Sorensen, Inc., ABAQUS USERS' Manual, 1990.

10. Gurson, A. L., Trans. ASME, Series H, *J. Eng. Mater. Tech.*, **99** (1977) 2.

11. Kuhn, L. T. and R. M. McMeeking, "Power Law Creep of a Junction Under Combined Shear and Pressure," in progress. 1991.

12. Richmond O. and R. E. Smelser, Alcoa Technical Center Report (1984).
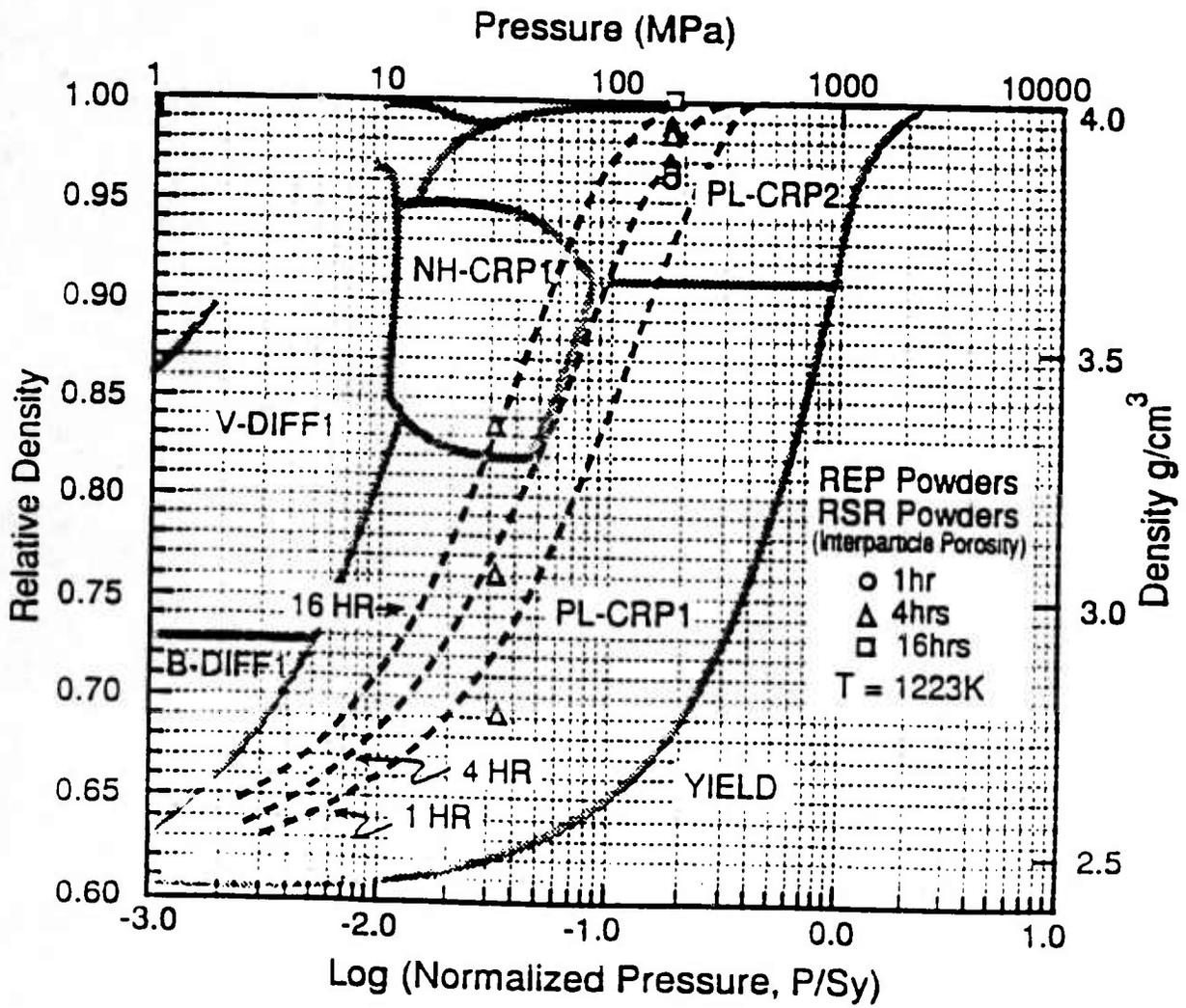
Figure 1: HIP Map for TiAl Powder
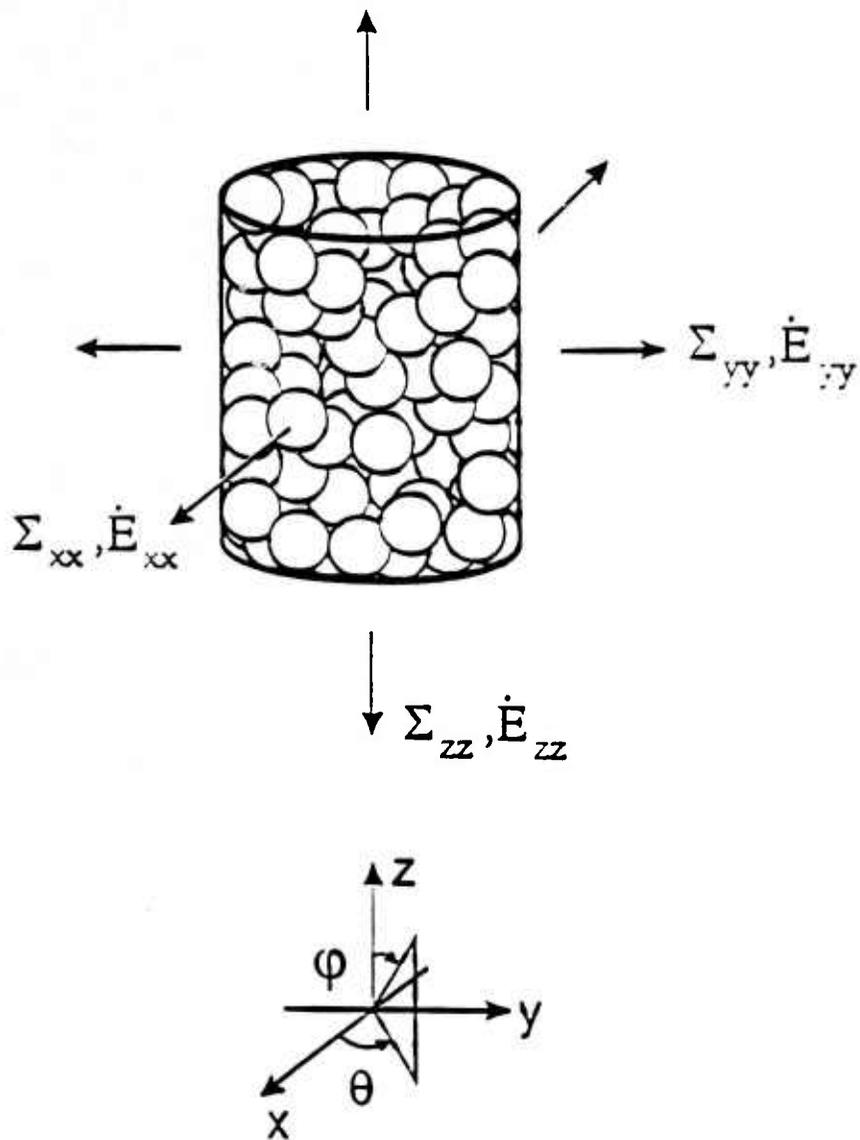
**Figure 2:** A Macroscopic Element of Powder Under Remote Axisymmetric Loading
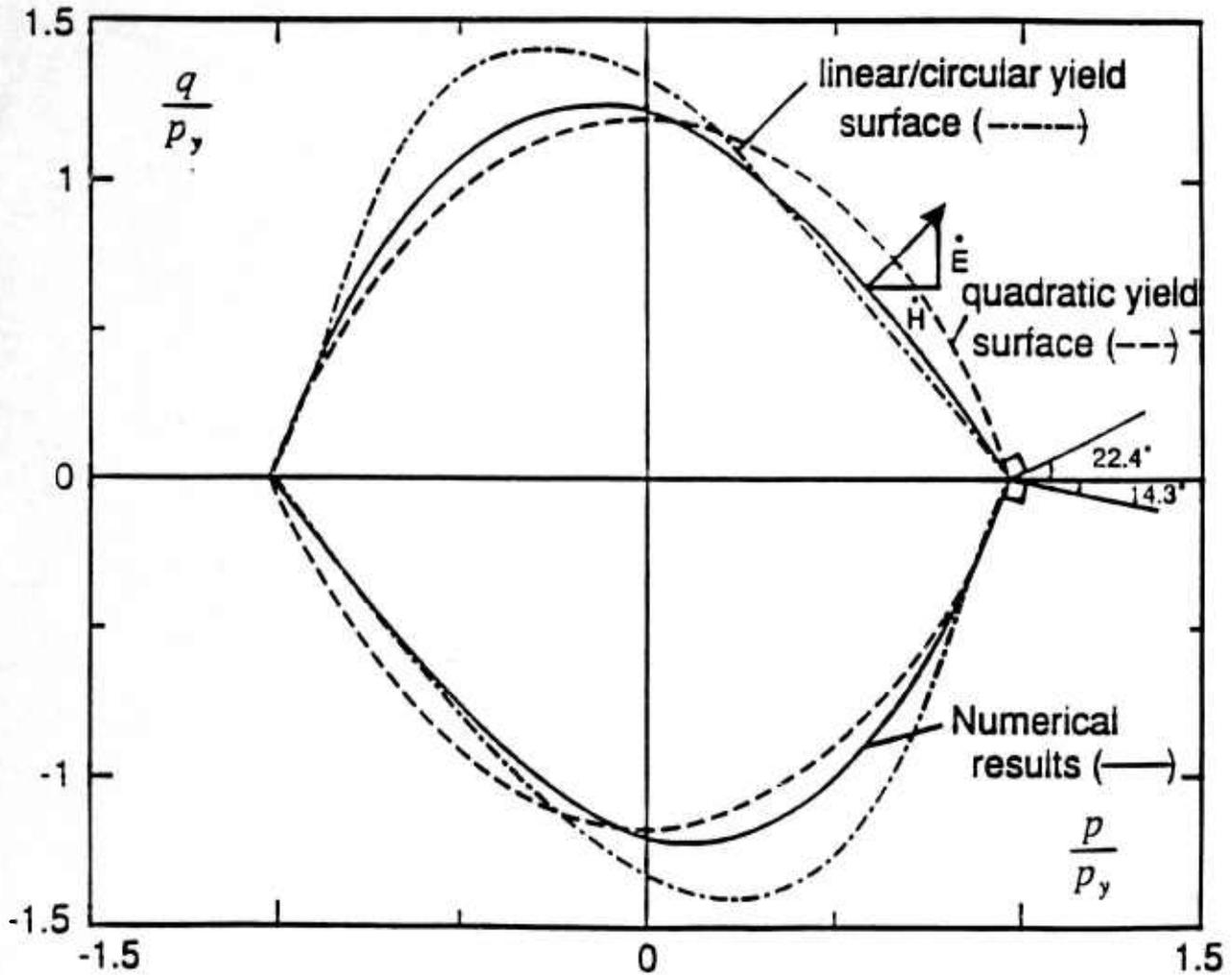
Figure 3: Yield Surface for Axisymmetric Loading of an Isotropic Homogeneous Packing of Rigid Perfectly Plastic Spheres
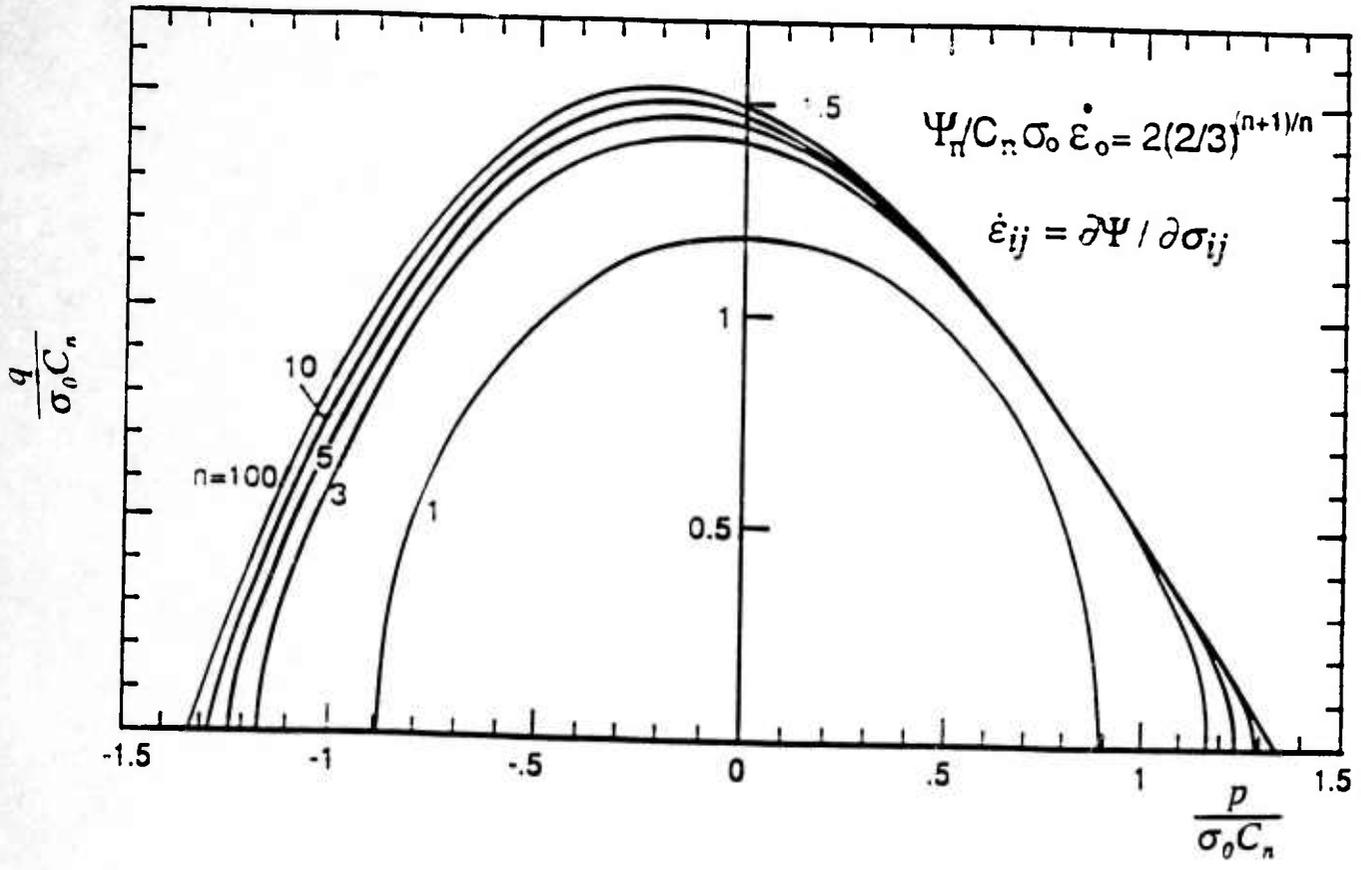
Figure 4: Flow Contours in Stress Space for which the Stage I Power-Law Creep Potential Estimate is a Constant
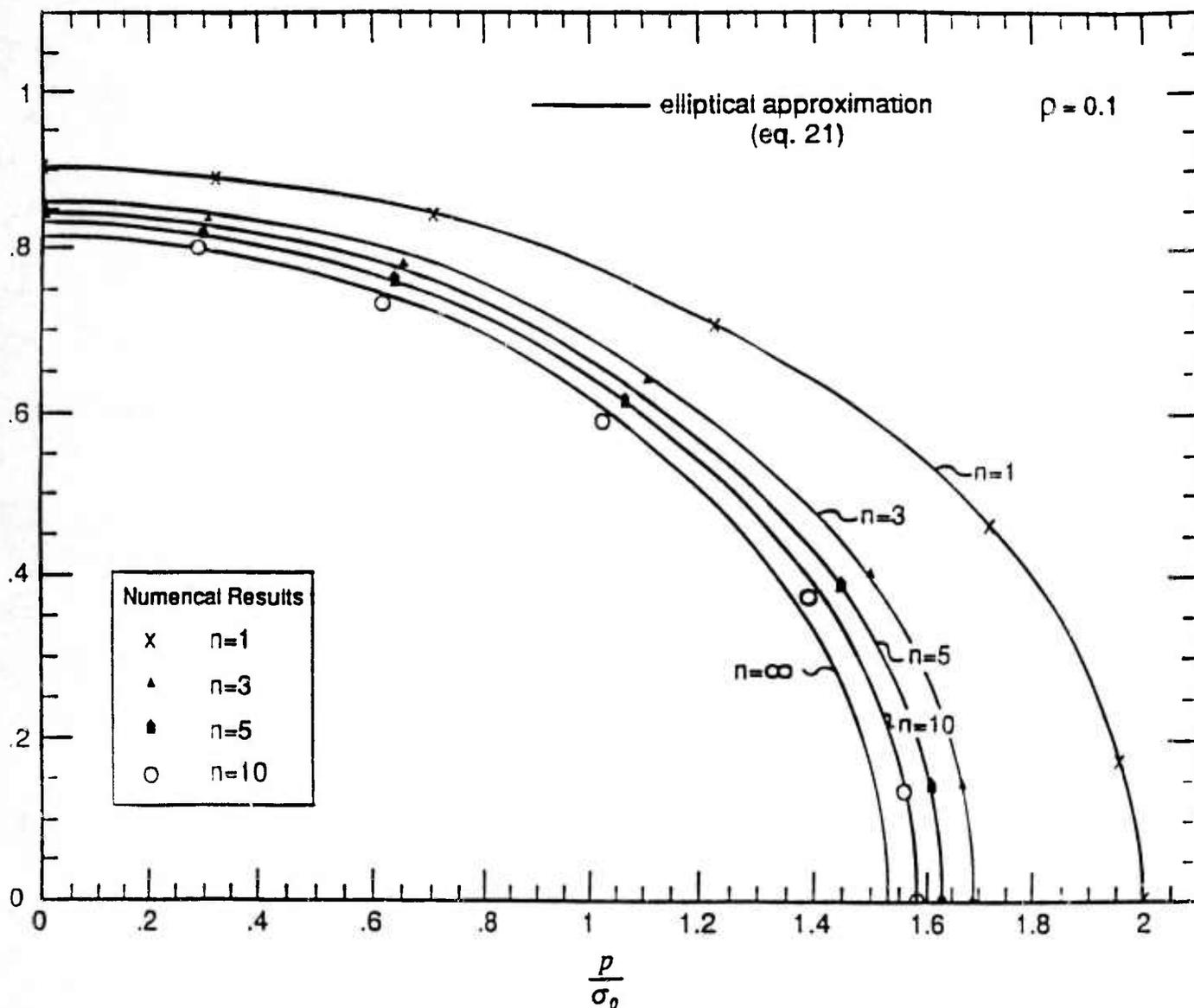
Figure 5: Flow Contours in Stress Space for which the Stage II Power-Law Creep Potential Estimate is a Constant

24

BDM FEDERAL, INC.

TOPIC 2: INTELLIGENT CONTROL OF CONSOLIDATION AND SOLIDIFICATION PROCESSES

Norman M. Wereley, Tony F. Zahrah and Frank H. Charron, BDM Federal, Inc.

Intelligent Processing of Materials (IPM) involves the integration of process models and *in-situ* sensors into an intelligent process controller to achieve desired material properties. BDM has developed IPM systems for both consolidation and solidification processes. This paper explores the application of models based on the finite element method to develop process actuation systems, to design process schedules, and component shape, and to develop a control model with which to control the process.

1.0 Introduction

Intelligent Processing of Materials (IPM) involves active control of a material process using analytical or empirical models and *in-situ* sensing of critical product features and process parameters to modify process schedules to meet pre-defined product goals. IPM involves the integration of three enabling technologies: process modeling, *in-situ* sensing, and intelligent control. BDM is leading IPM technology development teams for powder consolidation, and vertical Bridgman (VB) crystal growth involved in:

(1) Development, implementation, experimental validation, and application of process models;

(2) Development, and installation of *in-situ* sensors; and

(3) Development and implementation of control algorithms for closed-loop control.

Process models include high-fidelity FEM-based models, and reduced-order models. The application of FEM-based computational methods to the modeling and control of advanced material processes has been discussed in the literature. FEM-based models are used to predict the time evolutionary behavior during HIP [Zah92,Zah93], bulk crystal growth [BDM93a], plasma spray [Wei89,Bac90], and many other material processes. FEM-based models can also be used to determine the optimum process conditions, design the process schedules (such as furnace thermal profile, pressurization, and heating rates), identify critical areas for sensor placement, and assist in the design of process equipment. However, a primary advantage of an FEM-based approach is in the development of real-time feedback control strategies based on the FEM model.

A key parameter dictating performance of an intelligent control system is the control interval. The control interval is the duration during which all sensor measurements are obtained, model predictions are performed, control algorithms are executed, and commands are sent to the

process actuators to effect changes in a process schedule. The control interval is typically selected between 10 and 20% of the fastest time constant of the process. In general, the control interval for a typical advanced material process is much shorter than the time in which an FEM model can be executed to predict the same process behavior. To be included in a model-based control system, the process model must be able to predict process behavior in real-time. This leads to the notion of the reduced-order model, a model that is sufficiently simplified and accurate, to permit real-time prediction.

This fundamental trade-off between high-fidelity models and reduced-order models is explored for consolidation and solidification processes for which IPM systems have been developed by the authors. Near-net shape forming of powder materials using Hot Isostatic Pressing (HIP) required the development of an IPM system to make on-line assessments of how consolidation is proceeding, and to take any control actions (changes to the pressure and temperature schedules) needed to return the process to the desired processing path. The IPM system required (1) the development and application of process models for powder consolidation, (2) the use of eddy current sensors to monitor shape change during consolidation, and (3) the development of adaptive PID and model-based intelligent control strategies for consolidation.

The goal of IPM-based directional solidification of CdTe bulk crystal using the VB growth technique is to increase the single crystal yield, and control stoichiometric uniformity. The basic growth process involves relative translation of a quartz ampoule filled with unrefined molten CdTe through a temperature profile that includes its solidification temperature. A prototype industrial VB reactor was designed and assembled, and an IPM system for real-time monitoring and process control of CdTe bulk crystal growth was developed. The IPM system required the development and application of (1) a crystal growth model for conductive, radiative, and convective heat transfer mechanisms in the VB growth system, (2) *in-situ* sensors to monitor ingot conductivity, and the shape and location of the solidification front, and (3) adaptive control of material properties, ingot temperatures, and solidification front shape and location by modifying the thermal profile and/or translation rate of the furnace.

2.0 Intelligent Control of HIP

BDM has installed the first complete IPM system for HIP at Naval Air Warfare Center, and has successfully consolidated metallic and intermetallic powders under closed-loop control to achieve pre-defined goals. This goal required the development of process models, implementation of eddy current sensor technology, and development of intelligent control strategies.

BDM FEDERAL, INC.

2.1 Process Modeling

Although the process of consolidation is continuous, it is helpful to think of consolidation as occurring in three stages. The initial stage, referred to as Stage 0, is dependent on powder size distribution and component shape, as well as several pre-consolidation steps, including encapsulation, and binder burnout. Consolidation includes two stages. In Stage 1, voids within the material are interconnected, and deformation is concentrated at interparticle contacts. As relative density increases, the interparticle contact area increases until most of the interconnected voids are sealed off. The material, with isolated voids, is now in Stage 2.

BDM has worked with Cambridge University, University of California at Santa Barbara, and University of Pennsylvania on the development, implementation, and validation of constitutive models for consolidation of powder materials subjected to three-dimensional stress states [Kuhn91, Govi92, Zah93]. The micromechanics, mechanism-based models have been implemented in a general purpose finite element program. The numerical integration scheme uses a rate-dependent formulation to allow coupling of all densification mechanisms, applies to three-dimensional stress states, and allows the use of a coupled heat transfer-stress analysis solution algorithm. This PROcess SIMulation, PROSIM™, computer program can now be used to perform simulation for different process cycles, and the results will identify the active densification mechanism(s), and the contribution of each mechanism to densification.

To illustrate the application of these models to simulate the consolidation process and demonstrate their usefulness, computer simulations of two HIP experiments described by Li, Ashby and Easterling [Li87] were performed. In these experiments, steel canisters with torroidal shape were filled with tool-steel powder and HIPed under two different temperature and pressure schedules, as illustrated in Fig. 1. Canister deformation or shape change was observed in one experiment, while no shape change was observed in the other experiment. The deformed shapes obtained through numerical simulations [Zah92] agree with the experiments, as illustrated in Fig. 1. An examination of the analysis results illustrated in Figure 2 show that for the case in which shape change occurred, the plastic yielding mechanism was active early during consolidation. Power-law creep is dominant during the latter stages of consolidation. For the case in which no shape change occurs, power-law creep is the only active mechanism. These results illustrate the importance of process schedule and encapsulation design. Without a canister, no shape change occurs in specimens of this size (about 1 inch in thickness by 2 inches in height). In thick specimens, temperature gradients can result in non-uniform densification and shape change. The temperature gradients obtained during the computer simulations were less than 10 K. The results explain the source of shape distortion, which is mechanism-based, and illustrates the advantage of

27

BDM FEDERAL, INC.

mechanism-based models. Shape change is the result of the mechanisms that were active during consolidation.

2.2 In-situ Sensors

Of crucial importance to the ultimate success of closed-loop IPM system for HIP is the implementation of *in-situ* sensors from which process states can be either directly sensed or inferred. Estimates of sample density are required during HIP to control the consolidation process effectively. Two eddy current sensors were developed to monitor the changes in canister dimension, and to provide estimates of part density. The estimates of powder compact density can then be used to adjust process schedules in the event that consolidation is not progressing as expected.

The two types of eddy current sensors are a global (or encircling) sensor, and a local (or probe) sensor. Substantial engineering has been performed to harden these two eddy current sensors to survive the hostile environment inside a HIP chamber.

2.2.1 Global (or Encircling) Sensor

The global eddy current sensor non-destructively monitors key electrical features of a sample during the HIP process, from which reliable estimates of the sample diameter can be calculated. The global sensor consists of two coils. A primary coil which encircles the HIP sample, and to which an electrical excitation, or stimulus, is applied, and a secondary coil which is concentrically aligned to the interior of the primary coil, at the center of the longitudinal axis. The secondary coil picks up an electrical signal, or a response, that is proportional to the diameter of the sample inside the secondary. The resulting stimulus-response pair is used to calculate a frequency-dependent impedance curve. Effects of noise, lead placement, etc. can be eliminated by normalizing this impedance curve with respect to an impedance curve derived from an empty sensor. This temperature compensated normalized impedance curve is the basic data set used in all of the estimation techniques.

2.2.2 Local (or Probe) Eddy Current Sensor

The local eddy current sensor non-destructively monitors key electrical features of a sample during the HIP process, from which reliable estimates of the distance between the sensor and sample can be calculated. The probe sensor also uses a primary and secondary coil configuration, although of a different geometry from the global sensor. The probe sensor has greater flexibility

due to the wider variety of possible mounting configurations. Shape features can be measured by appropriately placing sensors around the sample on mechanically- and thermally-stable mounts.

2.3 Intelligent Control

The Intelligent Control System (ICS) for HIP is a UNIX-based Supervisory Control and Data Acquisition (SCADA) system enabling an operator to design, execute, and control HIP process schedules. It consists of three software modules: a process design module, a process control and data acquisition module, and a data analysis module.

The process design module uses PROSIM™ or PDT™ to generate candidate process schedules (process inputs such as temperature and pressure schedules versus time), exercise process models, and predict consolidation. Depending on the component shape and size (which affect the size of the finite element mesh), PROSIM™ may require more time and computer resources than available on-line during HIP. By assuming a uniform stress state, a reduced-order model suitable for embedding in a real-time control system can be derived. The stress state will vary depending on the consolidation process and part complexity. For HIP of a right circular cylinder, a hydrostatic stress state is the simplifying assumption used to produce a suitable reduced-order model. Reduced-order models for different stress states have been implemented in PDT™, a Process Design Tool.

The process control and data acquisition module executes process schedules developed with PDT™ and/or PROSIM™, and controls processing variables such as temperature, and pressure. It executes supervisory control, estimation, and low-level control strategies for HIP. Supervisory control monitors key process parameters, determines if the process goals are achievable, and modifies the process schedules, if required. Estimation provides on-line estimates of key process variables that are not directly measured by *in-situ* sensors. Existing estimators use eddy current sensor data to estimate internal temperature fields. Additional estimators are under development to estimate material properties that include yield stress and initial packing density. Low-level control utilizes control strategies, such as PID and fuzzy logic, to track the process schedules.

The data analysis module provides tools for the analysis and graphical representation of eddy current sensor impedance data collected during processing. Software tools are provided to replay the entire process database, manipulate the data, and create new process schedules for subsequent HIP cycles.

BDM FEDERAL, INC.

The IPM system provides off-line process planning using either PROSIM™ or PDT™, to produce process schedules consisting of a reference temperature, pressure, and density trajectories. Feedback control techniques are then used to track the reference trajectories, as illustrated in Figure 3. The objective of the on-line IPM control strategy is to track the reference density trajectory by minimizing density tracking errors. If the measured density undershoots the reference density trajectory, then the controller increases temperature and pressure, which softens the material and increases densification rate. Conversely, if the measured density overshoots the reference density trajectory, then the controller decreases temperature, and reduces densification rate. The authority to control the HIP process is shared between an off-line process design, and an on-line feedback control strategy.

The IPM system uses PID compensation to track density. PID is a non-model based control approach, which refers to a control strategy that does not execute a real-time model to determine a control action. After the density tracking error is compensated by the PID controller and checked against HIP equipment constraints, the resulting temperature correction is added to the reference temperature. The pressure change is a function of temperature according to a non-ideal gas law relationship.

2.4 Application to a CP Ti part

Closed-loop control of density was demonstrated for a one-inch diameter can of CP Ti (PREP) powder. The HIP cycle was designed to maintain a relatively constant rate of densification from the initial packing density to the desired final density. The off-line process schedule design anticipated data from temperature, pressure, and global eddy current sensors. Relative density was calculated based on diameter estimates obtained from the eddy current sensor. A thermodynamic model of the chamber represented the non-ideal Argon gas law. The reference temperature, pressure, and density trajectories, illustrated in Figure 4, were developed using PDT™, in conjunction with the chamber model. Note, however, that the reference pressure trajectory was purposefully designed to be too aggressive for this HIP chamber to emphasize the benefits of feedback control. The basic stages of the HIP cycle were as follows: cold pressurization, heating, temperature soak, and cooling. The HIP cycle starts with a cold pressurization to 36 MPa (5.3 ksi) at 373 K (100°C), then ramps to 1000 K (727°C) and a pressure of 75 MPa (11 ksi), and holds for 20 minutes before finally free cooling. The objective of the closed-loop control system for this HIP run is to track the reference density trajectory shown in Figure 4.

BDM performed the closed-loop HIP run using the reference trajectories shown in Figure 4. The actual (measured) temperature and pressure trajectories were obtained from on-line HIP

30

chamber monitoring. The actual (measured) density trajectory was obtained on-line from the global eddy current sensor. The control trajectory portrays the temperature and pressure set points sent to the PID loops controlling the HIP chamber temperature and pressure. With no density trajectory error feedback, that is, open-loop control, the temperature and pressure control trajectories would be identical to their respective reference trajectories. However, when using feedback control, each control set point is determined as a function of the density tracking error. The difference between control and actual trajectories is governed by the pressure (pumping and venting) capability of the HIP chamber.

The PID control strategy provided good density tracking performance for this CP Ti sample. The measured density tracked the reference density quite well, as illustrated in Figure 4. The first sign of a density tracking error occurred after the cold pressurization portion of the HIP cycle. This tracking error is due to the overly aggressive reference pressure trajectory. The ensuing oscillations in the actual density trajectory are due to a pressure shortfall at the end of cold pressurization, which was compensated by an increase in temperature. If the reference pressure trajectory were achieved by the HIP chamber, then the reference temperature and pressure trajectories would have produced the reference density trajectory.

2.5 Model-based Control

The FEM model is the model with the most fidelity in terms of accurate prediction of process behavior. To reduce the order of the model, assumptions are made on the process conditions, container shape, and physical properties of the material being HIPed. For example, by assuming a uniform stress state, a suitable reduced-order model can be developed and embedded in a real-time, intelligent control system. The stress state will vary depending on the consolidation process and part complexity. For HIP of a right circular cylinder, a hydrostatic stress state is the simplifying assumption used to produce a suitable reduced-order model.

To illustrate the application of the uniform stress state assumption, consider the model for Stage 1 power-law creep mechanism. The full 3D formulation is implemented in PROSIM™. By assuming a uniform hydrostatic stress state, the densification rate for Stage 1 power-law creep mechanism can be described by a non-linear ordinary differential equation (NLODE),

$$\dot{D}(t) = D(t)C_{cr}(t)P^n$$

where

$$C_{cr}(t) = \frac{27\pi}{16\sqrt{3}} B_{cr} \frac{(1-D_0)^{n-\frac{1}{2}}(D-D_0)^{\frac{1}{2}}}{\left[3D^2(D-D_0)\right]^n}$$

$$B_{cr} = \frac{A\mu b}{kT} D_{cr}\left(\frac{1}{\mu}\right)^n$$

$$D_{cr} = D_{0,cr}\exp\left(-\frac{Q_{cr}}{RT}\right)$$

Here, $\dot{D}$ is the densification rate, D is the current relative density, D_0 is the initial relative density, T is the temperature, P is the applied pressure, n is the creep exponent, Q_{cr} is the activation energy for creep, A is Dorn's constant, R is the universal gas constant, k is Boltzmann's constant, μ is the shear modulus of the fully dense material, and b is Burger's vector. These equations can be combined to yield

$$\dot{D}(t) = 3.1 B_{cr}(T) D \left(\frac{D-D_0}{1-D_0}\right)^{\frac{1}{2}}\left[\left(\frac{1-D_0}{D-D_0}\right)\frac{P}{3D^2}\right]^n$$

Each of the plasticity, creep, and diffusion mechanisms for both Stage 1 and Stage 2 can also be described by an NLODE. The states associated with HIP are density, $D(t)$, and grain size, $G(t)$. The control input variables are temperature, T, and pressure, P. The output variables are given by part temperature T_p, and density, $D(t)$, measured by the eddy current sensor, although additional output variables could be used if *in-situ* sensors were available. This model is in the right form to develop a model-based control strategy. One technique for developing a control model is based on linearizing the NLODEs that make up the process model [Wer93b]. Essentially, a nominal temperature and pressure trajectory is developed using PROSIM™. The resulting density and grain size trajectories are then calculated, which together with the temperature and pressure trajectories make up the process trajectory. The linearized model describes small perturbations of the nonlinear system about the process trajectory. The NLODEs that comprise the nonlinear model are then transformed to a set of time-varying linear equations, to which standard linear control system design tools can be applied. A gain-scheduled linear quadratic Gaussian control strategy is currently under development, and may improve density tracking performance of the HIP control system.

The non-model-based adaptive PID technique invests all control authority in process trajectory specification running off-line. The adaptive PID approach can only mitigate small deviations from the designed process trajectory by tracking the reference density trajectory. This

initial approach was taken to minimize the impact of unmodeled dynamics and parameter uncertainty that may have existed at the time the adaptive PID was implemented. As consolidation model validation proceeded, and these sources of error were reduced and/or eliminated, implementation of a model-based control strategy became feasible. Implicit in the model-based technique is the increase in real-time control authority that is implied by introducing a process model, and control algorithm running in real-time that can modify the process schedules. The model-based feedback control techniques should be able to deal with much larger deviations from the process trajectory due to sensor noise, and other disturbances. The details of this work-in-progress will be reported in a future paper.

3.0 Intelligent Control of Solidification

The primary objective of the intelligent control system for solidification is to demonstrate model-based, flexible manufacturing for directional solidification of infrared (IR) and other semi-conductor materials. To achieve this objective, a prototype vertical Bridgman (VB) reactor was built and tested. The prototype VB reactor was developed using the IPM approach, which combines process modeling and simulation, *in-situ* sensors, and adaptive control to achieve significant improvement in crystal producibility and product performance. In this section, some primary results from the first phase of an ARPA-sponsored program are described.

The intelligent VB reactor is intended to be extremely flexible, enabling production of multiple materials (CdTe:In, CdZnTe, InSb, etc.). CdTe materials have been used extensively in infrared electro-optic modulator applications due to its substantially higher modulation coefficient as compared to material systems such as GaAs. However, use of CdTe modulators has been severely restricted due to the extremely low yields of the processes used to produce this family of materials leading to extremely high price and unpredictability of deliveries. The CdTe family of materials is also used as IR substrates in HgCdTe growth.

The main process control objective is to produce a large single grain crystal. The primary source of yield loss is in the size of single crystal material. In this respect alone, this material lends itself to improvement using innovative IPM techniques to predict and control the crystal growth process. Although yield loss is primarily due to the size of single crystals, requirements to provide optimum modulation performance (high electrical resistivity, low absorption at the required wavelength, and resistance to breakdown under an applied electric field) provide a challenge to produce material of sufficient quality and with repeatability.

BDM FEDERAL, INC.

Application of IPM to the crystal growth of EO modulator material will improve process yields in two key ways: (a) dramatically improve single crystal yield, and (b) control the electro-optic properties of the material, especially resistivity, during the growth and cool-down phases of the process.

A schematic of the VB crystal growth system is shown in Fig. 5. The basic growth process involves relative translation of a quartz ampoule filled with unrefined molten material (CdTe or CdZnTe) through a temperature profile that includes its solidification temperature. This is done by either translating the furnace relative to the quartz ampoule, or by translating the temperature gradient along the longitudinal axis of the furnace, while holding furnace and ampoule stationary. In the industrial process, the quartz ampoule is stationary and the furnace translates. An important performance objective is to maintain predetermined longitudinal and radial temperature profiles. In some cases, composition of the melt can be controlled through Cd over-pressure generated by heating a Cd reservoir in the top of the ampoule (typically to a temperature of around 800 °C).

Three thermal profiles for VB growth are illustrated in Fig. 6. Existing VB reactors typically apply a parabolic thermal profile as shown at the far left. During the initial stages of this effort, a prototype 17 zone VB reactor capable of providing a flat thermal profile in the hot zone of the furnace was built. The gradients, G_1 and G_3, were set before growth. In the advanced VB reactor, the thermal profile shown at the far right, will have three gradients, G_1, G_2, and G_3, that can be actively controlled during growth.

The advantages of controlling these three gradients, especially G_3, will be explored. In addition, the use of an FEM process model to develop ampoule stand designs, furnace geometry, and control strategies will be discussed for CdZnTe crystal growth.

3.1 Process Modeling

Models for heat transfer, fluid flow, and stress analysis are under development for VB crystal growth. The lack of critical thermophysical properties hinders the accuracy of these models and the use of *in-situ* sensors as part of an IPM system. The key thermophysical constants required for proper modeling of VB crystal growth of CdZnTe can be grouped into three categories: thermal properties, physical properties, and optical, electrical, and magnetic properties. The thermal properties are required for analysis of heat transfer and fluid flow. The physical properties are required for stress analysis. The optical, electrical, and magnetic properties of CdZnTe in both the solid and liquid phases are required for *in-situ* sensor design.

Good estimates of pertinent physical properties for CdZnTe are necessary for modeling, sensing, and control applications. The property values are needed at both room temperature and at elevated crystal growth temperatures. At present, the published data set is incomplete, and most of the published properties are limited to room temperature.

Models used for analysis of VB crystal growth need to account for heat transfer and fluid flow, and must be able to calculate the stresses induced in the ingot. ABAQUS, a general purpose finite element code, was chosen to model heat transfer, including conductivity and radiation, and stress analysis. The results are used to give better understanding of the heat transfer problem, and to predict the shape and location of the solidification front.

3.2 Ampoule Stand Design

The first step was to analyze the current VB system illustrated in Fig. 7. The ampoule diameter was 55 mm. The VB configuration is axisymmetric with the axis of symmetry corresponding to the axis of revolution of the ampoule. As a result, the VB geometry can be modeled exactly using axisymmetric elements. Eight-noded, axisymmetric quadrilateral elements were used to generate the mesh. The mesh includes elements describing the mullite sleeve, quartz ampoule, CdZnTe mixture, ampoule stand, and stainless steel base. The model includes algorithms for calculating radiative heat exchange between the quartz and mullite, and the thermal interaction between the furnace and the mullite.

The calculations were aimed at supporting design of the ampoule stand. Key issues were identified and their effect on the shape and location of the solidification front were examined. The first key issue examined was the design of the ampoule stand, including geometry and thermal conductivity of the material. The ampoule stand was assumed to be a solid thick-walled tube, as in Fig. 7(a), or four concentric thin-walled tubes as illustrated in Fig. 7(b). The inner diameter of the central open core was assumed to be the same in both cases. The material choices for the ampoule stand were mullite (low conductivity material) or graphite (high conductivity material). For these calculations, the furnace temperature profile was assumed to be parabolic, as illustrated in Fig. 7(c). This temperature profile was used to define the thermal boundary condition at the outer surface of the mullite furnace liner.

To illustrate the effects of ampoule stand material and geometry, the thermal profile was positioned such that the CdZnTe melting temperature was within the conical base of the ampoule. The isotherms for this case are illustrated in Fig. 8. The steady-state heat transfer solution algorithm was used. The results provide the temperature distribution within the ampoule and support structure. The isotherm at the melting temperature (1366 K) gives the shape and location

BDM FEDERAL, INC.

of the solidification front. Based on the results, shape and location of the solidification front are strongly dependent on the choice of ampoule stand material, and weakly dependent on geometry of the ampoule stand.

Additional calculations were performed with the melting temperature at different locations inside the ampoule. The shape of the solidification front is nearly flat for an ampoule stand with low thermal conductivity (mullite), and highly convex for a base stand with high thermal conductivity (graphite).

The location of the solidification front is in the same horizontal plane as the location of the CdZnTe melting temperature in the furnace temperature profile for a base stand with low thermal conductivity material (mullite), and higher than the location of CdZnTe melting temperature in the furnace temperature profile for a base stand with high thermal conductivity material (graphite). This implies that a thermocouple measurement of the furnace liner is a poor indication of temperature inside the ingot.

The base stand material greatly affects the shape and location of the solidification front when the melting temperature in the furnace temperature profile is within the conical base of the ampoule. The effects diminish as the melting temperature moves into the cylindrical part of the ampoule.

3.3 Evaluation of the Furnace Design

Following these initial findings additional calculations were performed to support prototype furnace design. The prototype is a set of three Marshall type furnaces, mounted on a stepper motor driven vertical translation table, as illustrated in Figure 9(a). The ampoule diameter used in the prototype furnace is 75 mm. The temperature profile of the prototype furnace consists of three segments as illustrated in Figure 9(b). Two segments have a constant temperature, one segment below the melting temperature (cold section) and the other above the melting temperature (hot section). The thermal profile was maintained constant in the hot region to minimize convection. The third segment is a linear transition through the melting temperature, denoted by G_3. This temperature gradient, G_3, is the key process parameter to be evaluated in this analysis. Calculations were performed for five temperature gradients, namely, $G_3 = 4, 8, 12, 16,$ and 20 K/cm. Since the dependency of solidification front shape on ampoule stand geometry is weak, only the thick-walled tube ampoule stand results are shown. The material of the ampoule stand was assumed to be mullite, which has a low thermal conductivity as compared to graphite. The results for graphite are not shown.

BDM FEDERAL, INC.

Several positions of the furnace were considered. The corner of the ampoule is the location where the straight vertical line representing the ampoule wall transitions to the slanted wall of the conical ampoule bottom. A value of $z = 0$ denotes a position where the melt point in the temperature gradient, G_3, is coincident with the ampoule corner. Positive values of z are upward. Several values of z were considered: -4 cm, -2 cm, 0 cm, 2 cm, and 4 cm. The isotherm at the melting temperature (1366 K or 1093°C) of CdZnTe, gives the shape and location of the solidification front. A representative set of isotherms are shown for $G_3 = 4$ K/cm, 8 K/cm, 16 K/cm, and 20 K/cm for a position of $z = 0$. For $G_3 = 4$ K/cm, the solidification front is concave. As the gradient increases, the solidification front shape transitions through flat to increasing convexity, until convexity reaches a maximum for $G_3 = 20$ K/cm. A larger gradient, if practically feasible, could further increase the convexity of the solidification front.

Based on these results, an increase in ampoule diameter and a change in temperature profile from parabolic to linear combine to reduce the convexity of the solidification front. For an ampoule stand with low thermal conductivity, an increase in the temperature gradient from 4 to 20 K/cm causes the solidification front to transition from slightly concave to flat to slightly convex. For an ampoule stand with high thermal conductivity, an increase in the temperature gradient from 4 to 20 K/cm causes the solidification front to transition from nearly flat to slightly convex. Thus, by changing the applied gradient, the shape of the solidification front can be controlled. This is consistent with other research for horizontal Bridgman crystal growth [Dan91].

In some cases, the shape of the isotherms at the melting point exhibit waviness. A refined mesh is required for higher resolution of the solidification front shape. The model for concentric thin walled tubes does not presently allow for radiation between the tubes. These refinements will be included in the model once the design of the advanced prototype is frozen.

The process model developed in this study does not include convective coupling between the mullite sleeve and quartz ampoule. This effect appears to be small, but is a subject for future investigations. The results reported here are in-line with experimental observations during baseline crystal growth. Model validation will continue as *in-situ* sensor data becomes available. Once an *in-situ* sensor is available for integration in the furnace, the modeling results will support the decision on the location of the sensor near the solidification front.

3.4   Intelligent Control

One of the key control objectives in this process is the control of the solidification front shape and location. Here, the approach that is currently under development is described. The convexity of the solidification front is strongly dependent on the thermal gradient, G_3, as

BDM FEDERAL, INC.

illustrated in Fig. 11. The Marshall type furnace is a resistive coil surrounded by a substantial amount of insulation, that is, a furnace with a very high thermal inertia, and cannot lose heat. As a result, the prototype furnace is very robust, but has poor controllability characteristics. By using a furnace with a low thermal inertia, the gradients in the furnace can be modified during growth.

The parameter Dz, shown in Figure 11(a), is defined as the vertical distance at the center of the ingot from the location of the melt temperature at the ampoule wall to the melt temperature location at the center of the ingot. If Dz is positive, then the solidification front is convex as seen from the melt zone. If Dz is negative then the solidification front is concave. A flat solidification front corresponds to $Dz = 0$. The results summarized in Fig. 11(b) show the dependence of solidification front convexity, as expressed by Dz, on location of the melting point in the thermal profile with respect to the ampoule, and thermal gradient, G_3. Based on preliminary stress analysis calculations, the parameter Dz is related to the stress field. If Dz is too high, then the stresses in the solid may become greater than the critically resolved shear stress and cause dislocations in the crystal lattice structure. If Dz is too low, then the heat transfer characteristics have become unfavorable, indicating that the heat flux through the ampoule bottom is too low to maintain a convex solidification front.

Therefore, one control strategy is to select a trajectory for Dz as a function of z based on a stress analysis calculation that minimizes the amount of material exposed to stress fields higher than the critically resolved shear stress, and maintaining that value of Dz during growth. The reduced-order model is then the curve relating gradient, G_3, to location of the melting temperature at the furnace liner to maintain Dz constant.

The operating curves in Fig. 11(b) provide some rules of thumb in designing such a trajectory using the mullite thick-walled ampoule stand. The solidification front will be concave for $z < -2$ cm unless a large temperature gradient is used ($G_3 > 13$ K/cm). Second, for $z > -2$ cm, a temperature gradient $G_3 \geq 8$ K/cm must be maintained, since a flat interface is developed for $z = 0$ and $G_3 = 8$ K/cm, and the curves flatten after $z = 2$ cm. Larger values of G_3 would be much more favorable for a convex solidification front. Interestingly, the choice of ampoule stand material with a larger value of conductivity would increase the range of z where a convex solidification front occurs, thereby improving the controllability of the solidification front control strategy.

An IPM system to control solidification front shape and location, as illustrated in Fig. 12, is under development. The feedback control loop involves using an IR radiometer (camera), with a telescopic zoom lens with short depth of field, and imaging software to detect the shape and location of the solidification front, and to map isotherms throughout the solidifying boule. The

curvature detected using the IR sensor is then used, in conjunction with the operating curves, to select the appropriate gradient to apply to the crystal growth system.

A second control strategy is suggested by these results. To improve the chance of higher single crystal yield, it makes sense to grow the crystal until solid about halfway up the cone, and arresting furnace translation. Since the solidification front is highly concave below $z = -2$ cm, poly-crystalline material may tend to form. Stopping at $z = -2$ cm, holding, and then restarting growth with a large thermal gradient, $G_3 > 12$ K/cm, will tend to produce conditions favorable for a convex interface, and a better chance of growing single crystal material. This *melt back* technique as suggested by these analyses, is currently being used by an industrial crystal grower.

The impact of material selection on controllability of the solidification front control strategy, and the impact of ampoule shape on solidification front shape is currently in progress.

4.0   Conclusions

Two techniques are discussed for generating a reduced-order control models from a high fidelity FEM-based model: simplifying assumption based on the physics of the problem, and discovering a key process parameter and developing a set of operating curves that can be embedded in a model-based controller.

4.1   Intelligent Control of Consolidation

Development of an IPM-based Intelligent Control System (ICS) for HIP relies heavily on a process model, PROSIM™, that accounts for consolidation mechanisms and their coupling, canister deformation, powder packing non-uniformities, temperature gradients within the specimen, and coupled thermal-mechanical behavior. Computer simulations and actual experiments show good agreement for a number of components. PROSIM™ can be used to design and optimize process schedules to meet pre-defined goals, such as final shape, relative density distribution, minimization of density gradients, and minimization of residual stresses. The ICS uses a reduced-order process model, PDT™, for process planning and on-line prediction of process behavior. The assumption of a uniform stress state was used to develop a reduced-order consolidation model for HIP. We plan to transition this model to fill the role of a real-time control model as the basis for gain-scheduled linearized LQG control strategy.

4.2   Intelligent Control of Solidification

FEM-based models incorporating conductive, convective, and radiative heat transfer, as well stress analysis, were used to improve the vertical Bridgman crystal growth process.

BDM FEDERAL, INC.

Guidelines for the fabrication of ampoule stands, furnace geometry, and solidification front control strategies were developed using the process model. The models can be used to minimize stresses induced by the thermal environment, as well as tailoring the thermal environment to achieve improved solidification front characteristics. The solidification front control strategy is based on a set of operating curves, or a look-up table, describing the effect of changing thermal gradient on solidification front curvature.

REFERENCES

[Dan91]   J.A. Dantzig, and L.S. Chao. "Interface shape control in Bridgman crystal growth." In Modeling of Casting, Welding, and Advanced Solidification Processes V, Eds. M. Rappaz, Mr. Ozgu, and K.W. Mahn, The Minerals, Metals, and Materials Society, 1991.

[Govi92]   S.M. Govindarajan. *Deformation Processing of Porous Metals*. Ph.D. Thesis. Dept. of Mechanical Engineering and Applied Mechanics, University of Pennsylvania. December, 1992.

[Kuhn91]   L.T. Kuhn, and R.M. McMeeking. "Constitutive models for powder compaction under non-hydrostatic stress states." Report prepared by University of Santa Barbara for BDM Federal, Inc., December 1991.

[Li87]   W.P. Li, M.F. Ashby, and K.E. Easterling. Acta Metallurgica, Vol. 35, No. 12, 1987.

[Wei89]   D.Y. Wei, D. Apelian, and B. Farouk. "Particle melting in high temperature supersonic low pressure plasma jets," *Metallurgical Transaction B*, Vol. 20B, April 1989, pages 251-262.

[Wer93a]   N.M. Wereley, and T.F. Zahrah. "Infrared Materials Producibility," Final Subcontract Progress Report, prepared by BDM Federal Inc. under ARPA contract MDA972-91-C-0046, May, 1993. Report no. BDM/VAS-0790-TR-93

[Wer93b]   N.M. Wereley, and T.F. Zahrah. "Linearization of the consolidation process model using a uniform stress state assumption", Technical Memo BDM/VAS-NMW-draft-93. January 1993.

[Zah93]   T.F. Zahrah, N.M. Wereley, F.H. Charron, and J.R. Mills. "Hot isostatic pressing using the intelligent processing of materials approach." In *Proceedings of the Hot Isostatic Pressing '93 Congress*, Antwerp, Belgium, 21-23 April 1993.

[Zah93]   T.F. Zahrah, C.J. Coe, and F.H. Charron. "The role of process models in intelligent hot isostatic pressing of powder materials." In proceedings of *Applications and Material Models to Design and Processing*, TMS, 4-5 March 1992.

FIGURES
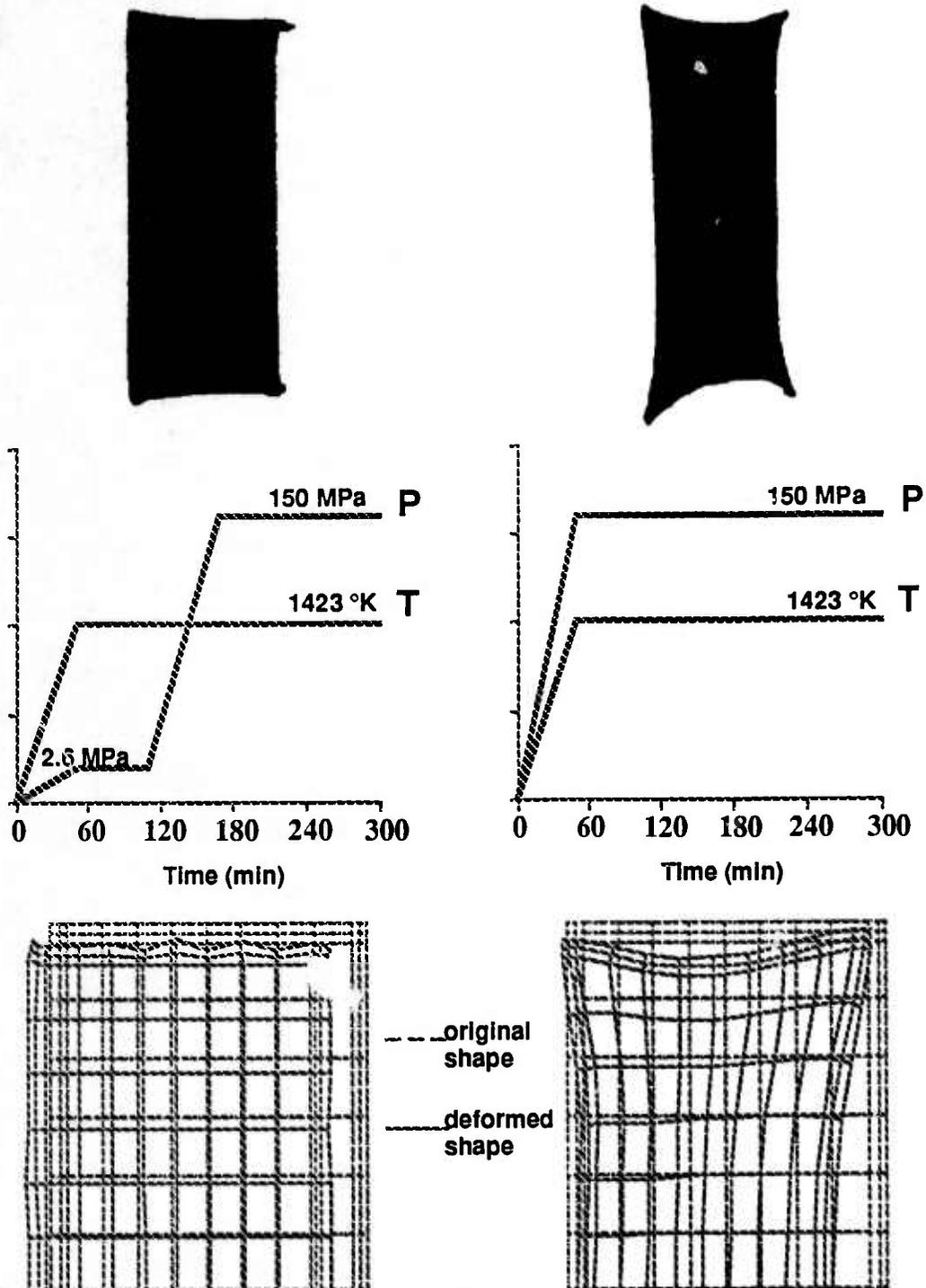
Figure. 1 Results from PROSIM™ are in agreement with experimental observations.

41
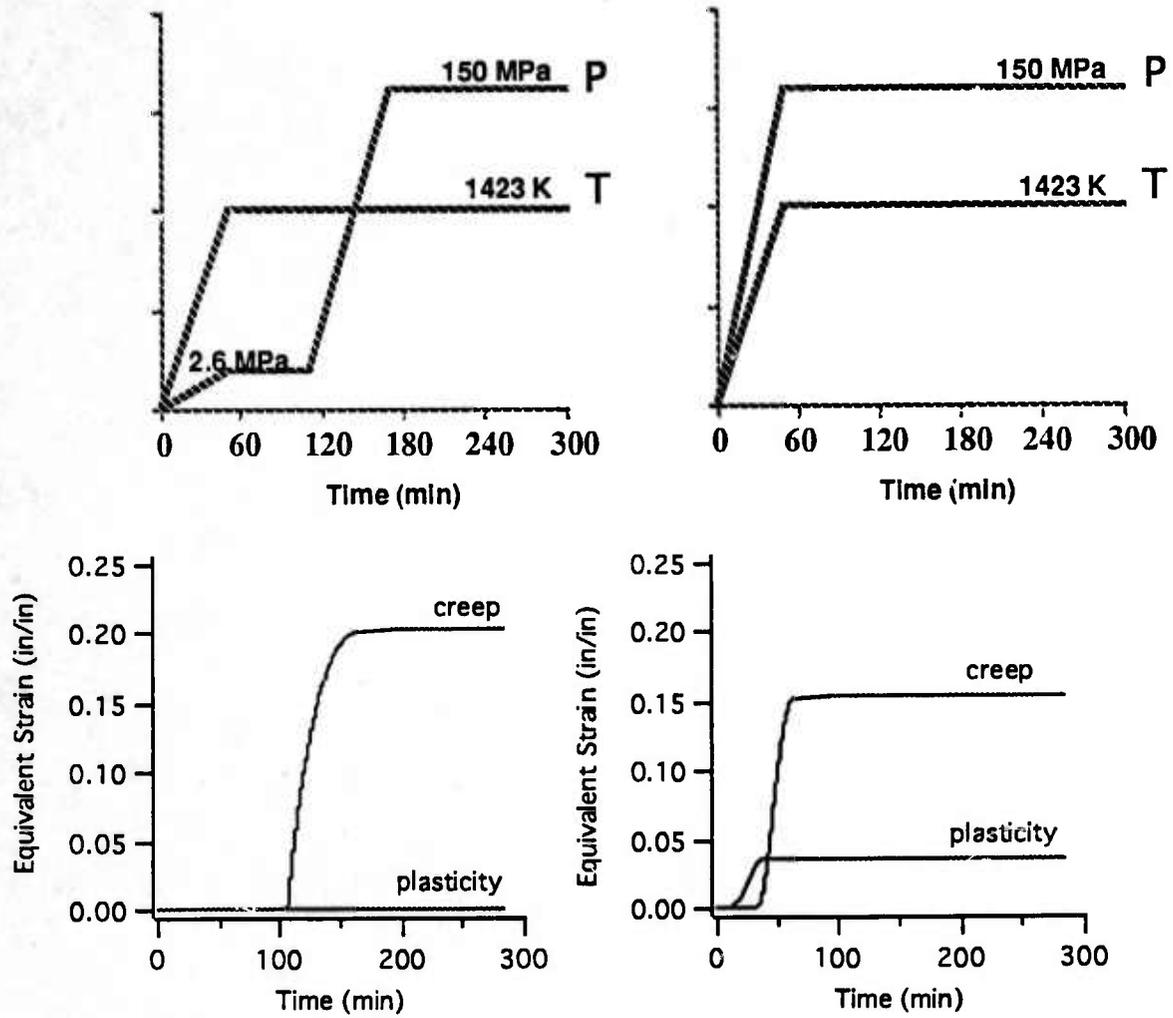
Figure. 2   Contribution of plastic yielding and power-law creep mechanisms to powder densification for the two HIP schedules .

BDM FEDERAL, INC.
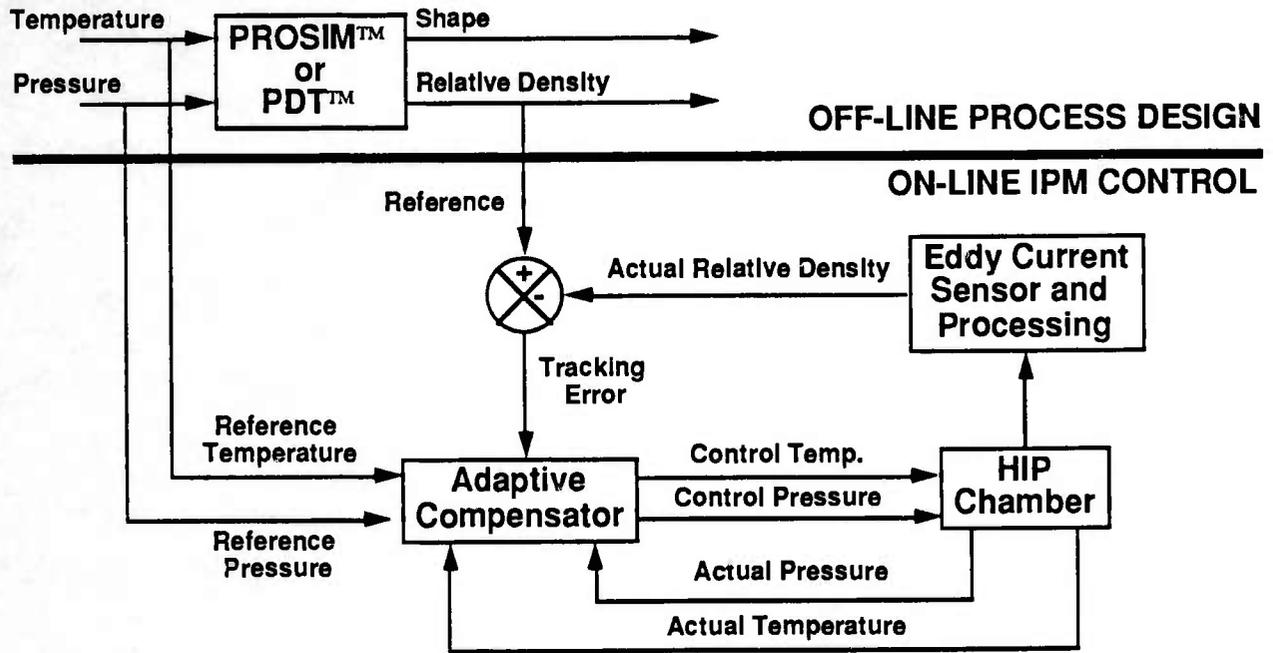
Figure. 3   The IPM-based Intelligent Control System for HIP uses off-line process design, and an on-line density tracking IPM control strategy based on reference trajectories for temperature, pressure, and density developed using the process design module, PDT™. Currently, an adaptive gain scheduled PID algorithm has been implemented. Future implementations will include a linearized LQG model-based compensation technique, and a fuzzy logic compensator.
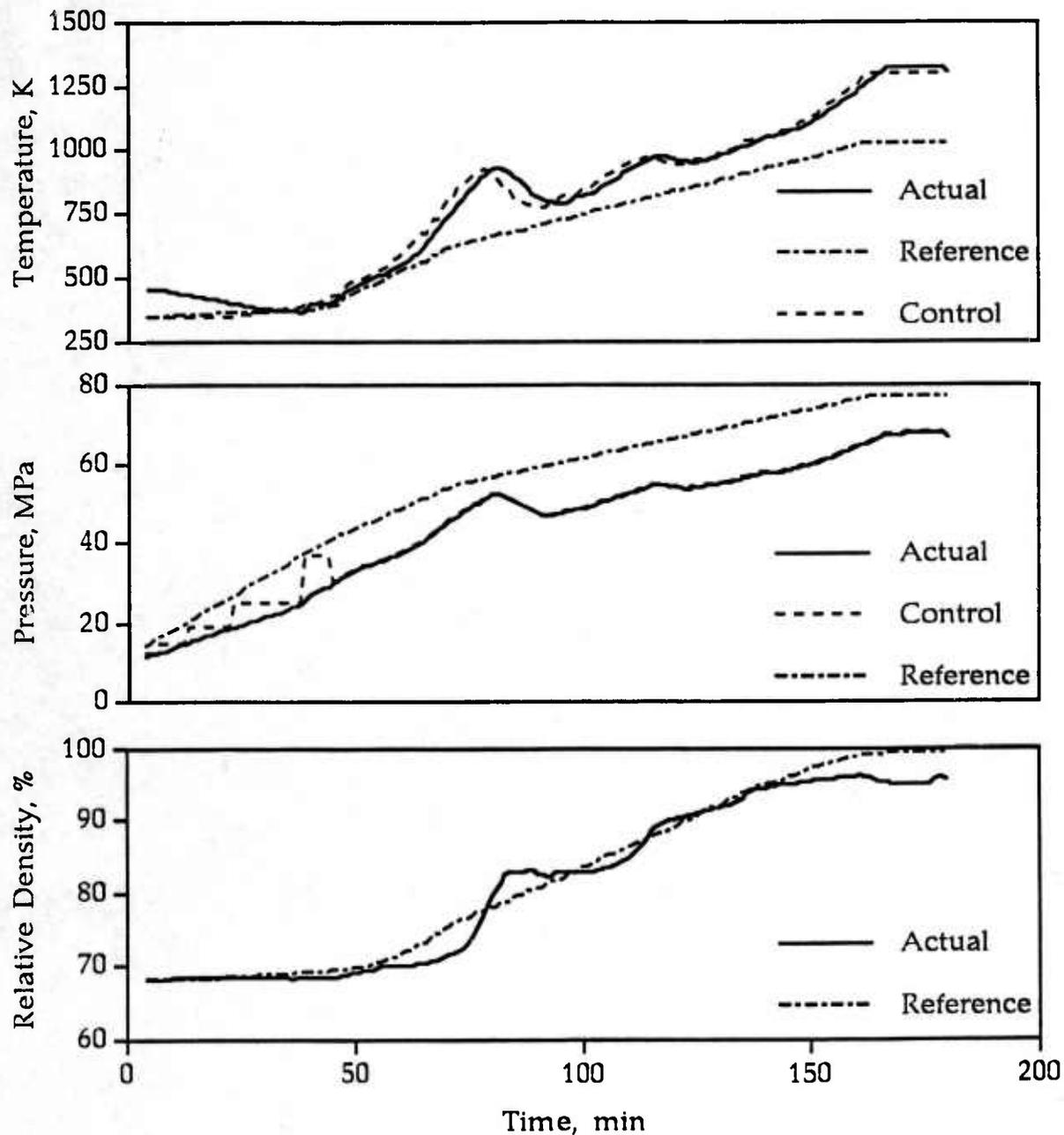
Figure. 4   Closed-loop control of a HIP cycle for CP Ti.
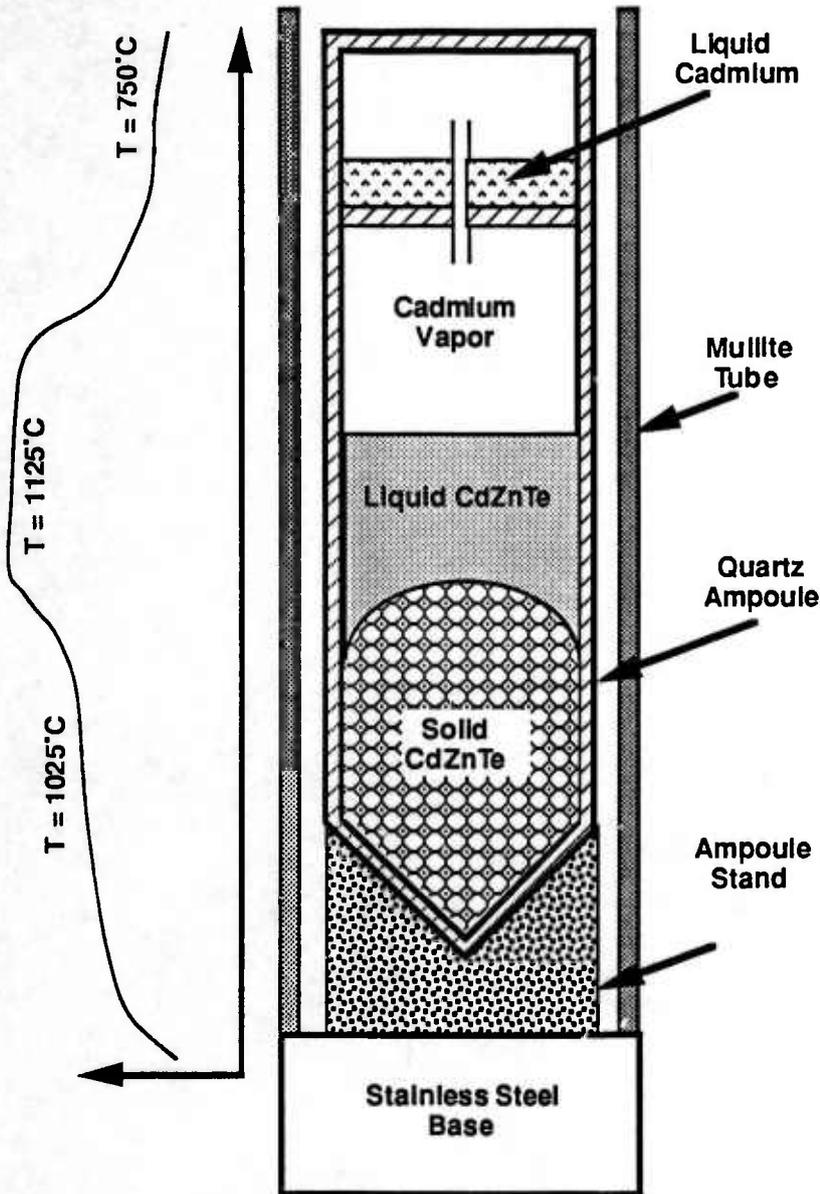
Figure. 5 Schematic of the materials and furnace configuration used to model the vertical Bridgman crystal growth process. A nominal axial thermal profile is illustrated in order to emphasize heat exchange aspects of the desired process models.
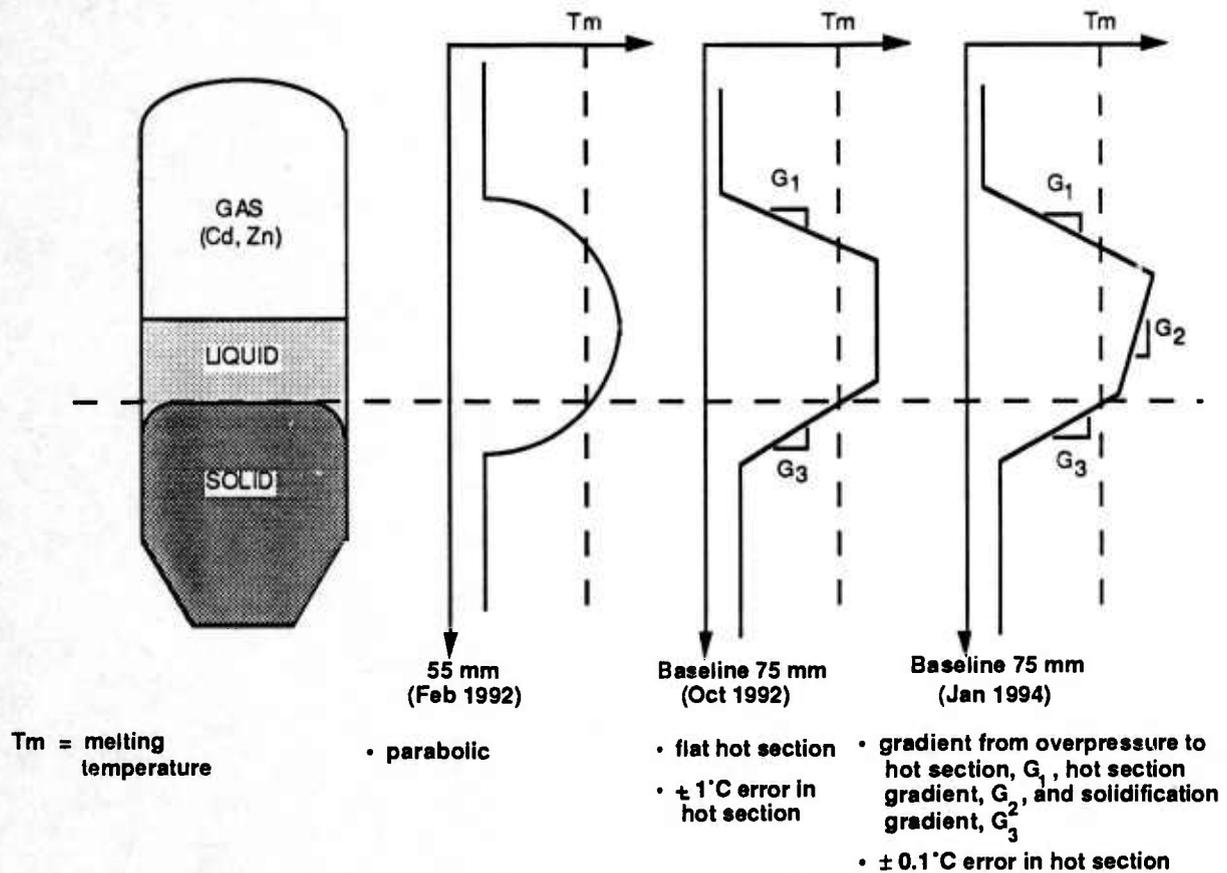
Figure. 6 Advanced thermal profile control. Existing industrial VB furnaces typically use a parabolic thermal profile. An improved industrial furnace design was developed to provide a flat thermal profile in the hot section, as shown in the second thermal profile. Transitioning to advanced thermal profile control will allow direct control of gradients G_1, G_2, and G_3, to vary process parameters that can be used for experimental model verification at minimal cost.
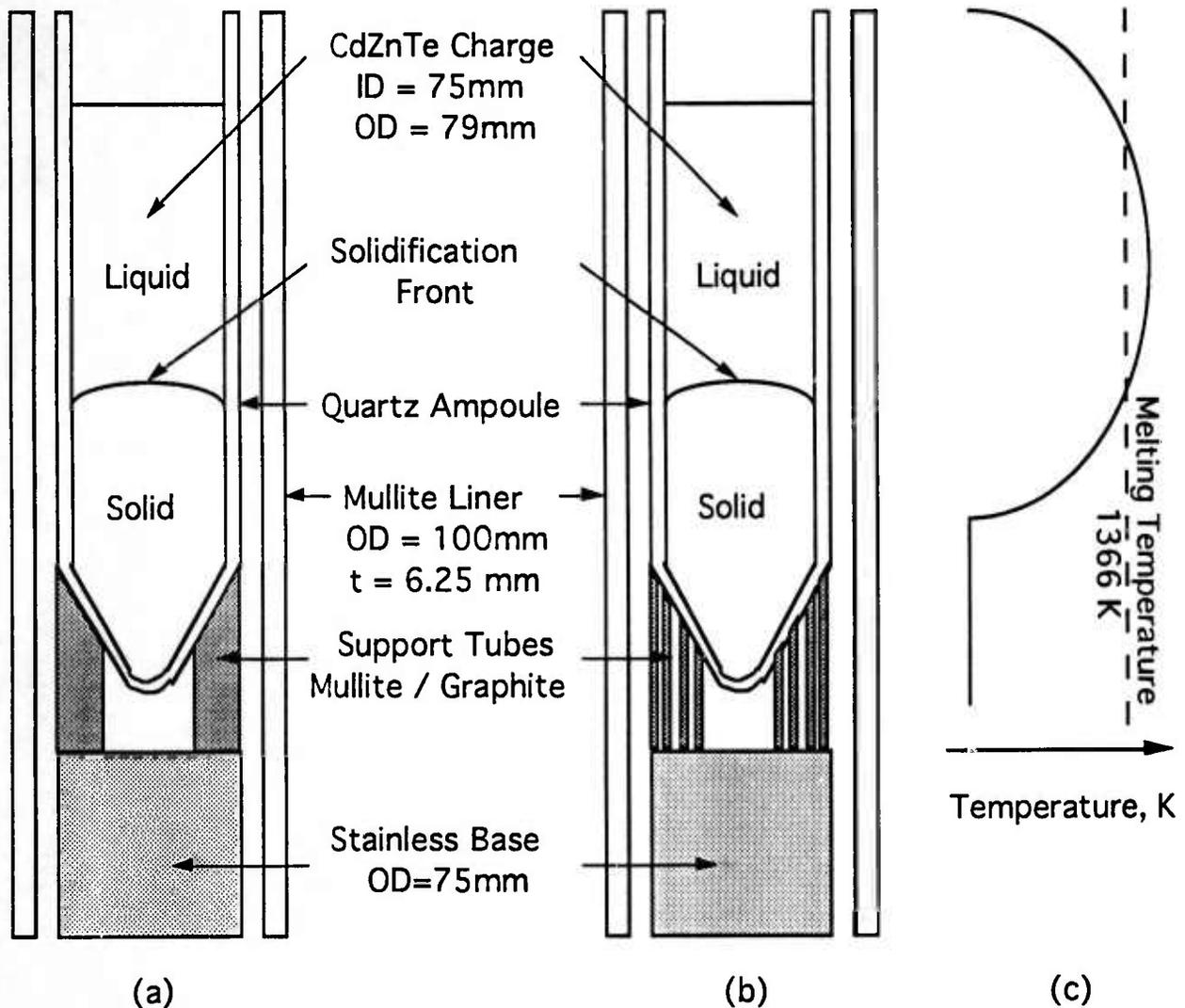
Figure. 7 Vertical Bridgman crystal growth reactor configuration. (a) Ampoule stand is a solid thick walled tube fabricated from either mullite or graphite with nominal OD = 75 mm and ID = 30 mm. (b) Ampoule stand is a series of four thin-walled tubes fabricated from either mullite or graphite with wall thickness t = 3.125 mm and spaced 3.125 mm apart. (c) Nominal parabolic thermal profile used to evaluate performance of the ampoule stand configurations.
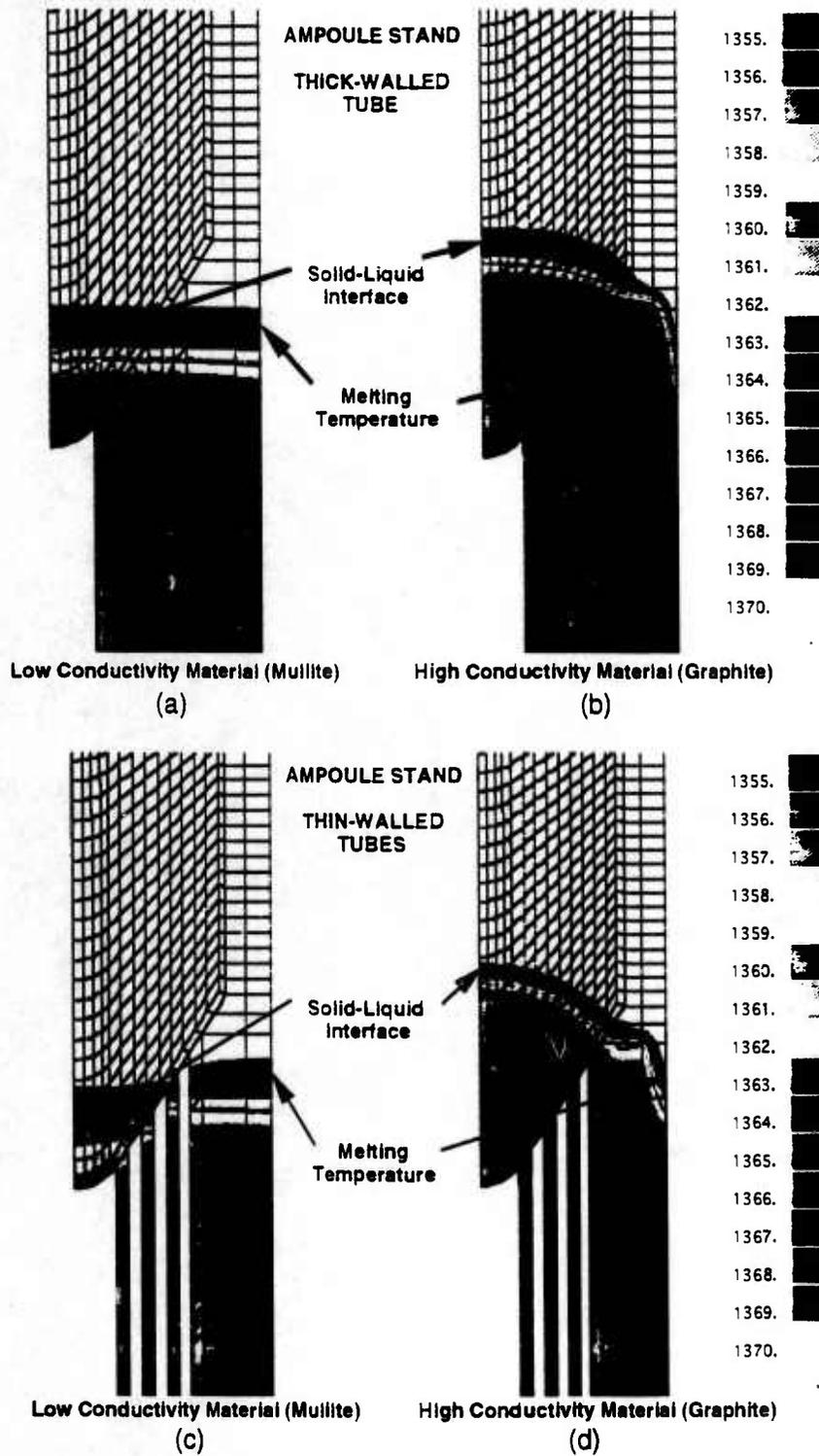
Figure. 8 Isotherms for vertical Bridgman configuration with melting temperature positioned within conical base of ampoule. Results show that solidification front curvature is strongly dependent on ampoule stand material and weakly dependent on ampoule stand geometry. (a) Ampoule stand is a thick-walled mullite tube. (b) Ampoule stand is a thick-walled graphite tube. (c) Ampoule stand is a series of thin-walled mullite tubes. (d) Ampoule stand is a series of thin-walled graphite tubes.

48
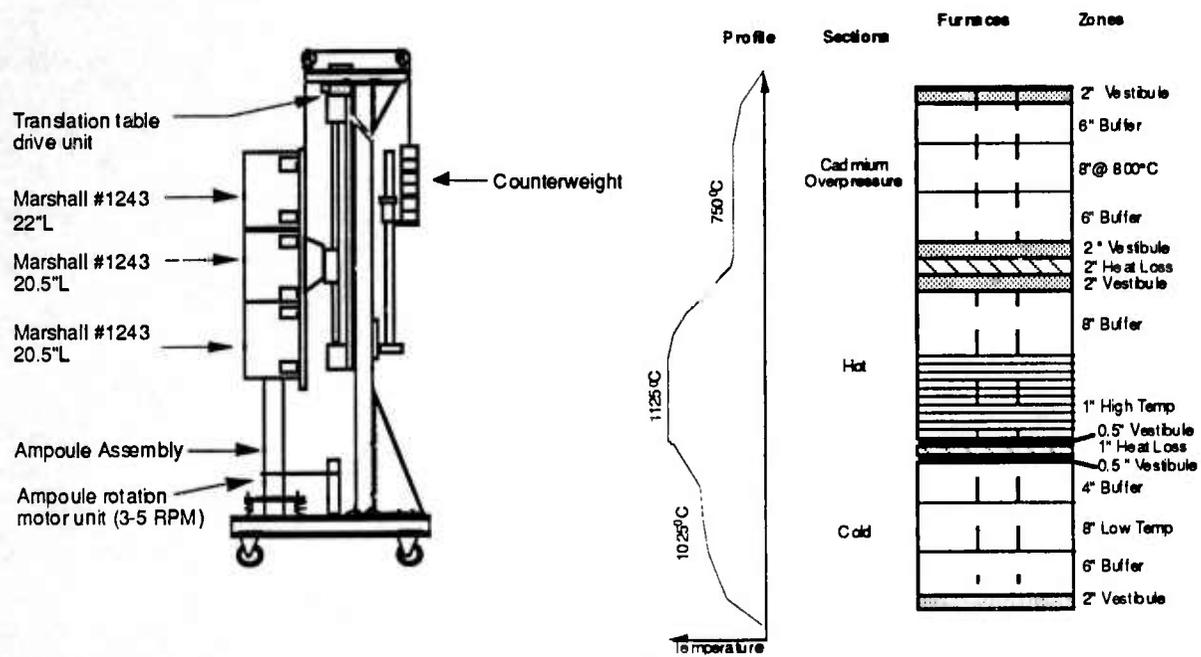
(a) Furnace frame

(b) Furnace geometry

Figure. 9   Prototype vertical Bridgman reactor configuration.

(a) Gradient, G3 = 4 K/cm

(b) Gradient, G3 = 8 K/cm

(c) Gradient, G3 = 16 K/cm

(d) Gradient, G3 = 20 K/cm
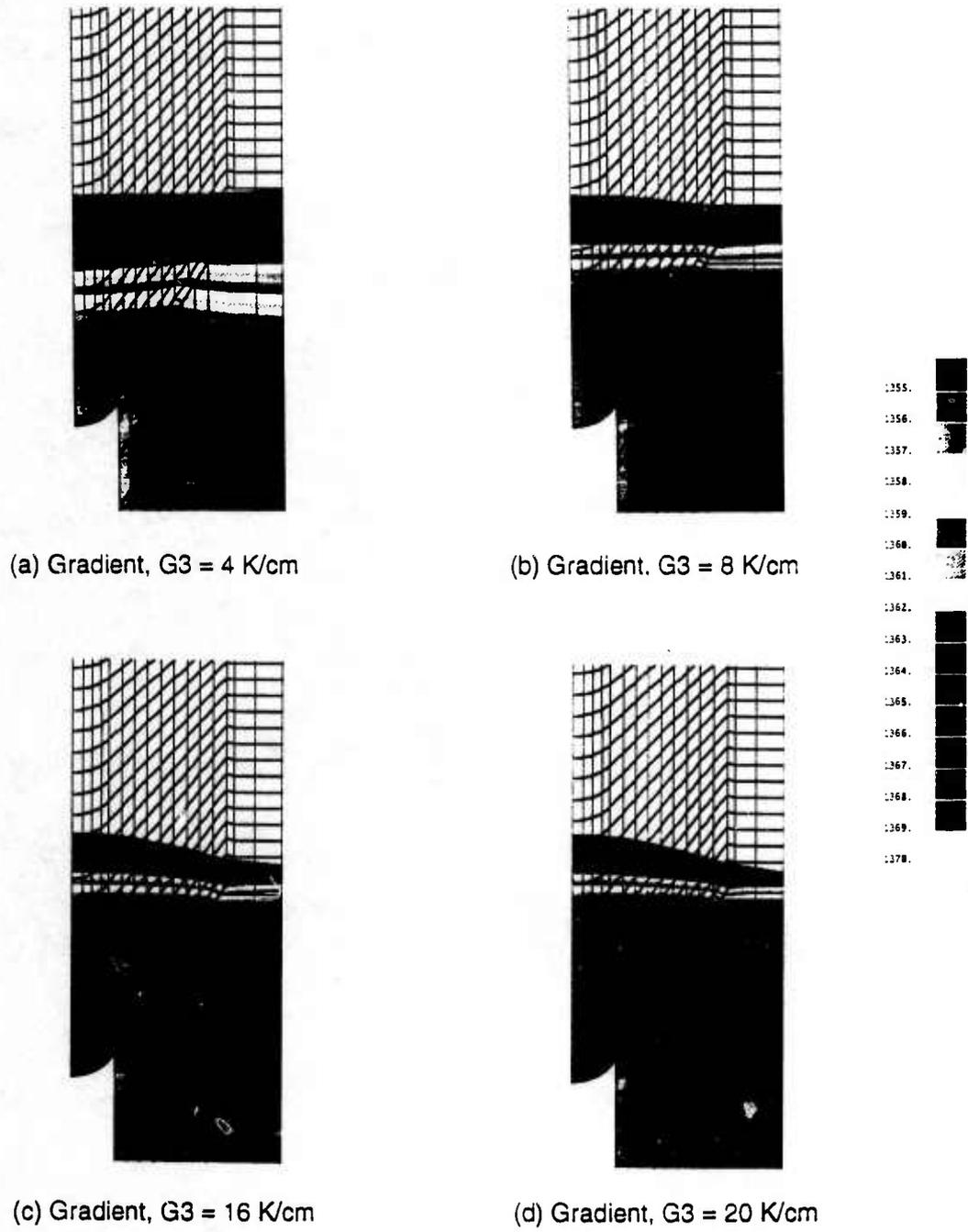
Figure. 10 Isotherms for a vertical Bridgm. n configuration with a solid thick-walled ampoule stand and a melting temperature positioned at top of the conical base of the ampoule ($z = 0$). Four different values of temperature gradient, G_3, are shown.
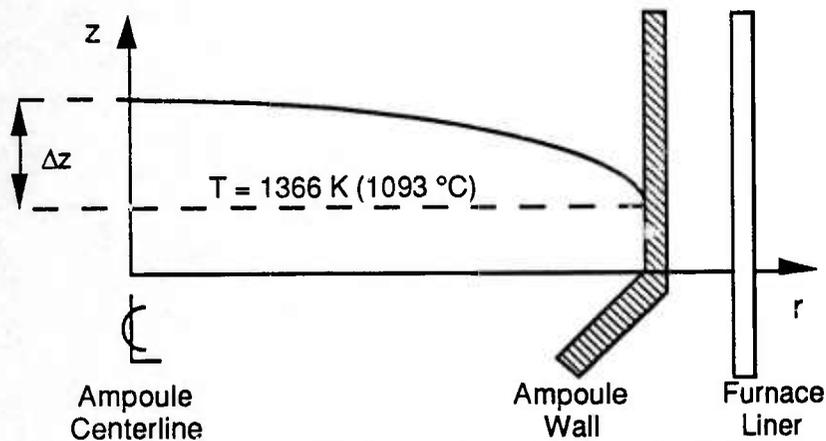
(a) Definition of convexity, Dz, and melting point location, z..
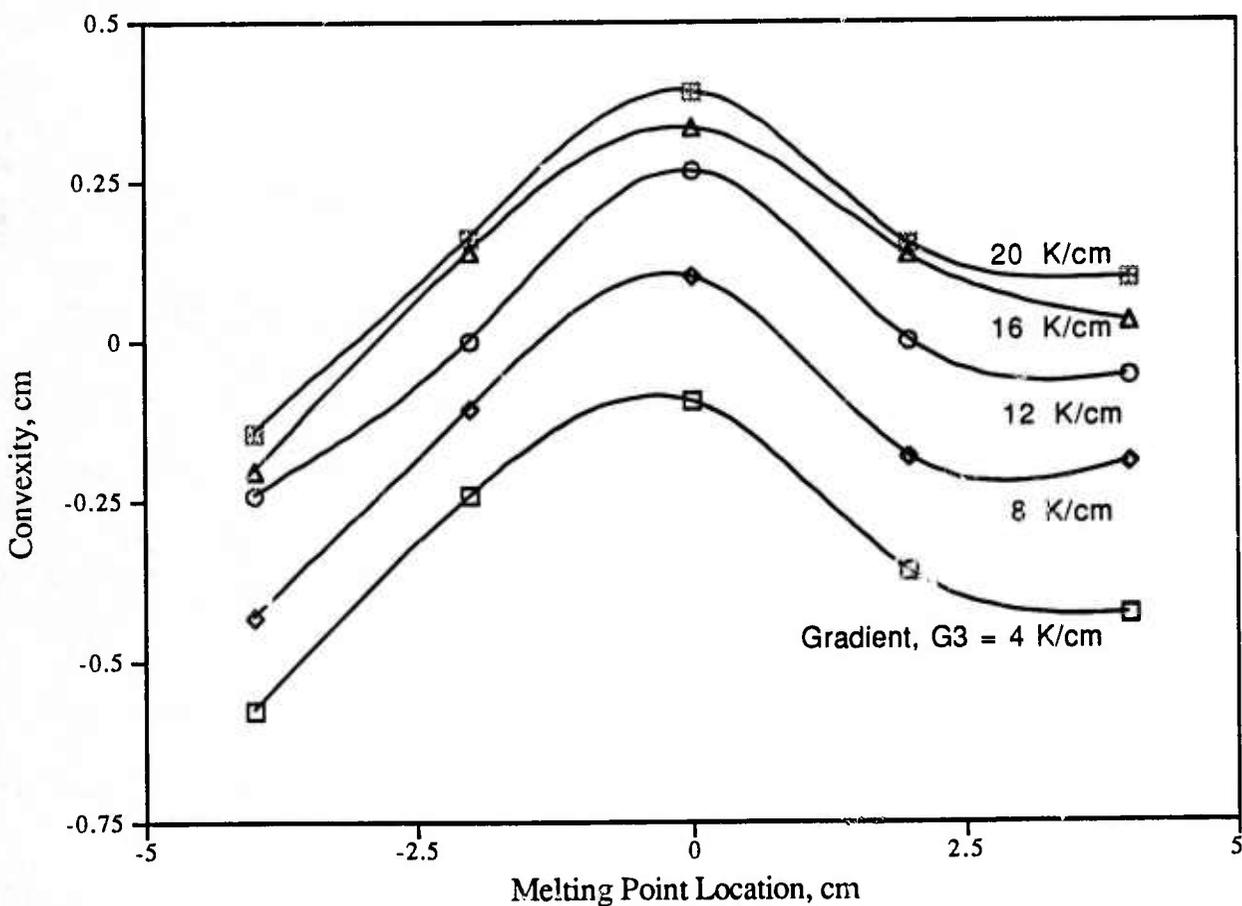
(b) Operating curves for solidification front control

Figure. 11 Operating curves for solidification front shape control. (a) Definition of convexity, Dz, and melting point location, z. (b) Trajectories for solidification front shape control showing convexity, Dz, versus melting point location for different values of the thermal gradient, G3. Control of solidification front location is achieved through thermal profile position.
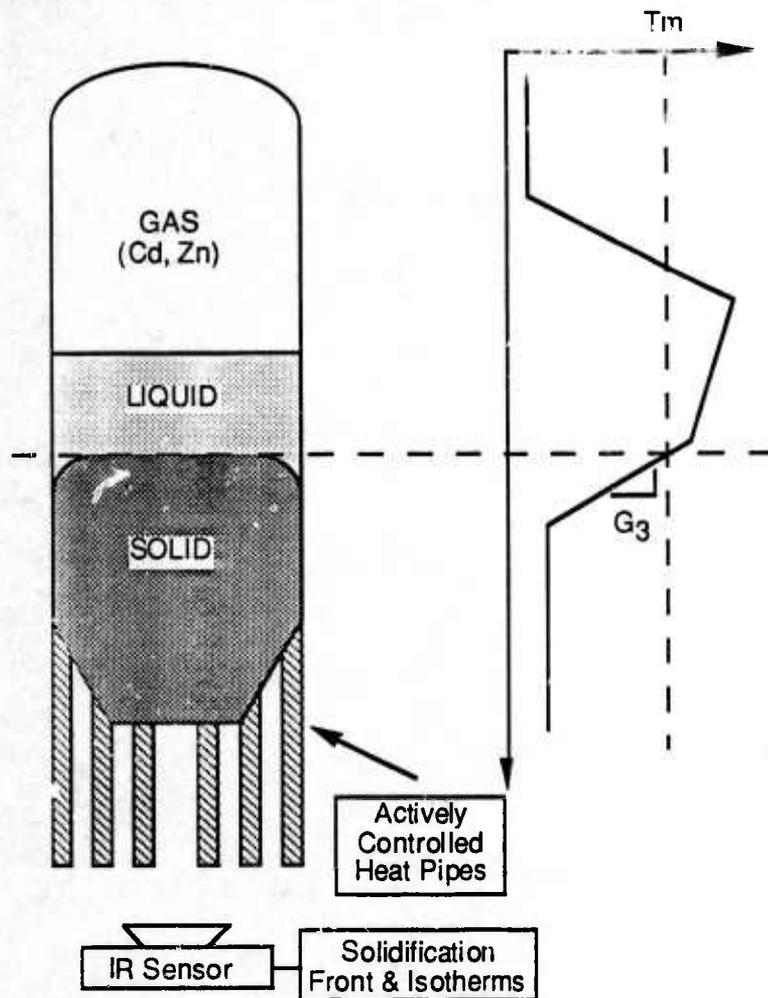
Figure. 12   IR sensor (camera), telescopic zoom lens with short depth of field, and imaging software, can be used to detect isotherms inside solidifying boule, as well as solidification front shape and location. This technique exploits the axisymmetry of the vertical Bridgman reactor.